Received: 29 March 2021 | Revised: 8 July 2021 | Accepted: 25 July 2021

DOI: 10.1111/bre.12599

RESEARCH ARTICLE

Basin Research | IAS EAGE | WILEY

Integrated source rock evaluation along the maturation gradient. Application to the Vaca Muerta Formation, Neuquén Basin of Argentina

J. B. Spacapan[1] | **M. Comerio**[1] | **I. Brisson**[2] | **E. Rocha**[3] | **M. Cipollone**[1] | **J. C. Hidalgo**[4]

[1]YPF-Tecnología S.A. (Y-TEC-CONICET), Buenos Aires, Argentina

[2]YPF S.A., Buenos Aires, Argentina

[3]Pluspetrol S.A., Buenos Aires, Argentina

[4]Schulmberger GmbH, Aachen, Germany

Correspondence
J. B. Spacapan, YPF-Tecnología S.A. (Y-TEC-CONICET), Av. del Petróleo Argentino (RP10) S/N, Berisso (CP 1923), Buenos Aires, Argentina.
Email: juan.b.spacapan@ypftecnologia.com

Abstract

The Vaca Muerta Formation (Tithonian–early Valanginian) is the main source rock in the Neuquén Basin and the most important unconventional shale resource in South America. In the present study, organic geochemistry, electron microscopy and basin and petroleum system modelling (BPSM) were combined to evaluate source rock properties and related processes along a transect from the early oil (east) to the dry gas (west) window. The unit is characterized by high present-day (1%–8% average) and original (2%–16% average) total organic carbon contents, which increase towards the base of the unit and basinal (west) settings. Scanning electron microscopy shows that organic pores derived from the transformation of type II kerogen. Isolated bubble pores are typical of the oil window, whereas bubble and densely distributed spongy pores occur in the gas stage, indicating that the maturity gradient exerts strong control on organic porosity. Organic geochemistry, pressure and porosity data were incorporated into a 2D basin petroleum system model that includes the sequential restoration of tectonic events and calculation of compaction trends, kerogen transformation, hydrocarbon generation and estimation of pore pressure through geologic time. The W–E regional model extends from the Agrio Fold and Thrust Belts to the basin border and allows us to evaluate the relationship between thermal maturity and timing of hydrocarbon generation from highly deformed (west) to undeformed (east) regions. Modelling results show a clear decrease in maturity and organic matter (OM) transformation towards the eastern basin margin. Maximum hydrocarbon generation occurred in the inner sectors of the belt, at ca. 120 Ma; long before the first Andean compression phase, which started during the Late Cretaceous (ca. 70 Ma). Miocene compression (15–7 Ma) promoted tectonic uplift of the inner and outer sectors of the belt associated with a reduction in thermal stress and kerogen cracking, as well as massive loss of retained fluids and a decrease in pore pressure. The OM transformation impacted (a) the magnitude of effective porosity associated with organic porosity development, and (b) the magnitude and distribution of pore pressure within the unit controlled by hydrocarbon generation and compaction disequilibrium. BPSM shows a progressive increase in effective porosity from the top

to the base and towards the west region related to the original organic carbon content and maturity increasing along the same trend. Overpressure intervals with high organic carbon contents are the most prone to develop organic pores. The latter represent favourable sites for the storage of hydrocarbons in the Vaca Muerta Formation.

KEYWORDS

hydrocarbon generation, modelling, organic porosity, pore pressure, thermal maturation, Vaca Muerta

1 | INTRODUCTION

Recognition of source rocks for oil and gas is the most critical risk element in petroleum exploration activities (Curiale & Curtis, 2016; Tissot & Welte, 1984). Source rock evaluation consists of assessing hydrocarbon generating potential, organic matter (OM) type, hydrocarbons that might be generated and thermal maturity (Dembicki, 2009; Katz, 1995; Tissot & Welte, 1984). Unconventional plays are usually analysed in terms of average total organic carbon (TOC) content, mineralogy, porosity, permeability, geomechanical properties and pore pressure (Ejofodomi et al., 2011; Hazra et al., 2019; Passey et al., 2010; Peters et al., 2017; Wang & Gale, 2009). At basin-scale, however, studies that focus on the assessment and quantification of these parameters are still scarce (Romero-Sarmiento et al., 2013).

Analytical techniques and numerical models including basin and petroleum system modelling (BPSM) packages are widely used tools to evaluate conventional and unconventional resources (Al-Hajeri et al., 2009; Hantschel & Kauerauf, 2009; McCarthy et al., 2011; Mei et al., 2021; Peters et al., 2017; Romero-Sarmiento et al., 2013). The analysis of unconventional resources based on estimation of burial temperature history and variations in maturity gradients allows simulation of a wide variety of geological processes through time, such as: (a) compaction trends, (b) transformation of OM by thermal maturity, (c) generation–retention–expulsion of hydrocarbons, (d) hydrocarbon composition, (e) overpressure and fracturing mechanisms and (f) preservation–development of porosity (Al-Hajeri et al., 2009; Burgreen-Chan et al., 2015; Grohmann et al., 2021; Hantschel & Kauerauf, 2009; Mei et al., 2021; Peters et al., 2017, 2018; Romero-Sarmiento et al., 2013; Tissot & Welte, 1984). Recent studies integrate BPSM tools with laboratory analysis to perform semi-quantitative descriptions of processes that control hydrocarbon generation, expulsion and retention capacity (Mei et al., 2021; Romero-Sarmiento et al., 2013, 2014). For instance, BPSM of the Mississippian Barnett Shale (Fort Worth Basin, USA) provided a quantitative means to estimate the total volume of generated hydrocarbons and the distribution of organic porosity at basin scale assuming that overpressure accompanied by diagenetic precipitation of cements inhibited the effects of compaction (Romero-Sarmiento et al., 2013). In that unit, model results and petrographic and analytical studies indicated that organic pores are formed by thermal stress and represent the main sites for hydrocarbon trapping (Loucks et al., 2009; Reed & Loucks, 2015; Romero-Sarmiento et al., 2014).

Highlights

- Evaluation of the Vaca Muerta Fm based on organic geochemistry, petrography and petroleum system modelling.
- Timing of hydrocarbon generation linked to tectonic events and burial depth.
- TOC content increases towards the base of the unit and basinal (west) settings.
- Organic pores developed from the early oil to the dry gas window derived from the transformation of type II kerogen.
- Hydrocarbon generation and compaction disequilibrium are the main mechanisms that generate pore pressure.

The Meso–Cenozoic Neuquén Basin in northern Patagonia is one of the most important hydrocarbon basins in South America (Legarreta et al., 2008; Uliana & Legarreta, 1993; Urien & Zambrano, 1994; Veiga et al., 2020) and, in recent years, it has become well known for its unconventional oil and gas resources (e.g. Badessich et al., 2016; Legarreta & Villar, 2011; Sagasti et al., 2014). The basin has three marine organic-rich source rocks known as the Los Molles, Vaca Muerta and Agrio formations (Fms). In particular, the Vaca Muerta Fm (Tithonian–lower Valanginian) constitutes a world-class source rock and an unconventional shale resource for both oil and gas (Brisson et al., 2020; Legarreta & Uliana, 1991; Legarreta et al., 2008; Veiga et al., 2020). In recent years, a great number of sedimentological, palaeontological, geochemical and stratigraphic works have been

reported for the unit (see Section 2). However, regional basin-scale modelling integrated with scanning electron microscopy (SEM), organic geochemistry and pore pressure measures has not been published.

In order to evaluate the source rock potential of the Vaca Muerta Fm (VMFm) through geological time, a transect in the central part of the Neuquén Basin (37° S) was analysed using a regional 2D petroleum system model that extends from the Agrio Fold and Thrust Belt in the west to the basin border in the east (Figure 1). BPSM involves sequential restoration of the deformation, calibrated by published thermochronological dating, which allowed us to integrate regional tectonic events and processes that controlled the thermal maturity and generation and expulsion of hydrocarbons. In addition, the present work incorporated key parameters, such as original total organic carbon (TOC_0) content, porosity and pore pressure conditions, in a basin simulator to test the magnitude and distribution of organic porosity (Øorg) and evaluate the causes of overpressure in the VMFm through the geological evolution of the Neuquén Basin. The characterization of such processes provides a partial evaluation of the unconventional potential of the unit. Such characterization, integrated with geomechanical properties, has a direct impact on the strategies of hydraulic fracturing (Peters et al., 2017).

Thus, the aims of the present article are to: (a) establish the original and present-day TOC distribution and transformation gradients for the VMFm at different basin positions (from dry gas to the early oil window) using a robust Rock-Eval® pyrolysis data set, (b) characterize the origin and types of organic pores (Øorg) as function of thermal maturation via high-resolution 2D-SEM, (c) obtain a semi-quantitative evaluation of the unit using 2D regional BPSM to test the timing of hydrocarbon generation–expulsion from the Fold Belt in the west to the basin border in the east and (d) test kerogen transformation into hydrocarbons, porosity development and the magnitude of pore pressure to evaluate the unconventional potential of the Vaca Muerta source rock.

2 | GEOLOGICAL SETTING

The Meso-Cenozoic Neuquén Basin (Figure 1), located in the Northern Patagonian Andes, extends between 32° and 40° S latitude, covering an area of 120,000 km^2 and includes parts

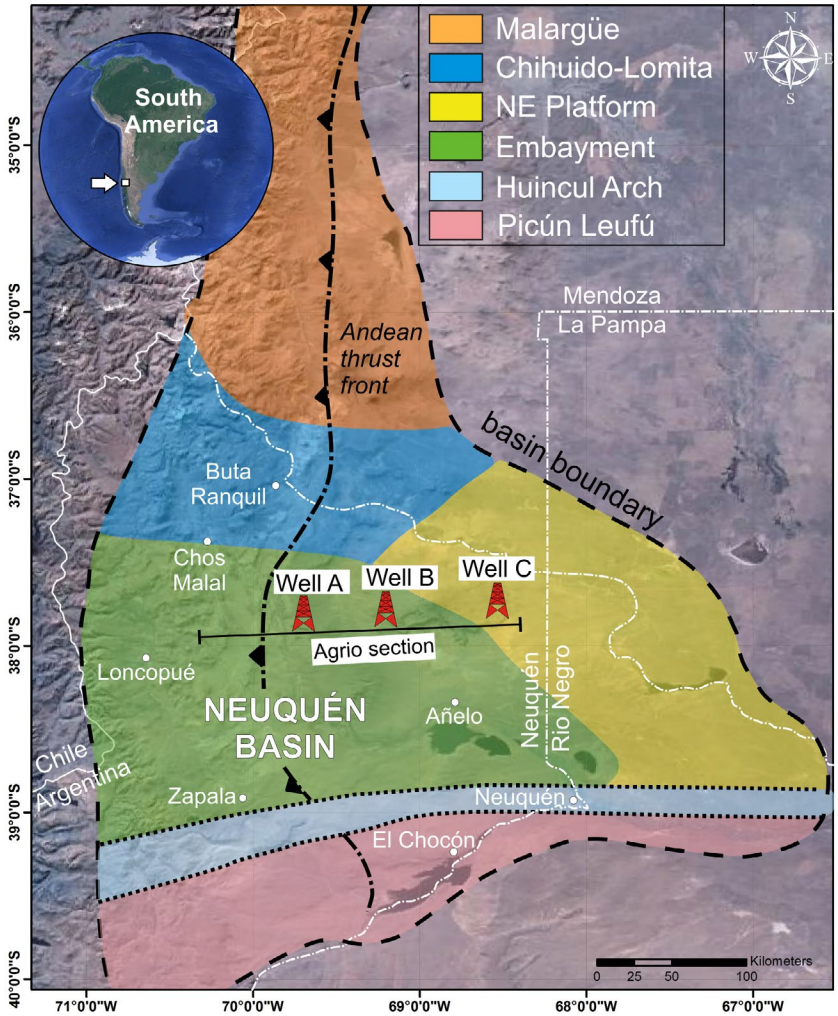

FIGURE 1 The Neuquén Basin of west-central Argentina. Satellite image showing the internal reference areas for the VMFm (Brisson et al., 2020) and the positions of analysed wells within the Agrio (Agrio-Section) fold and thrust belt

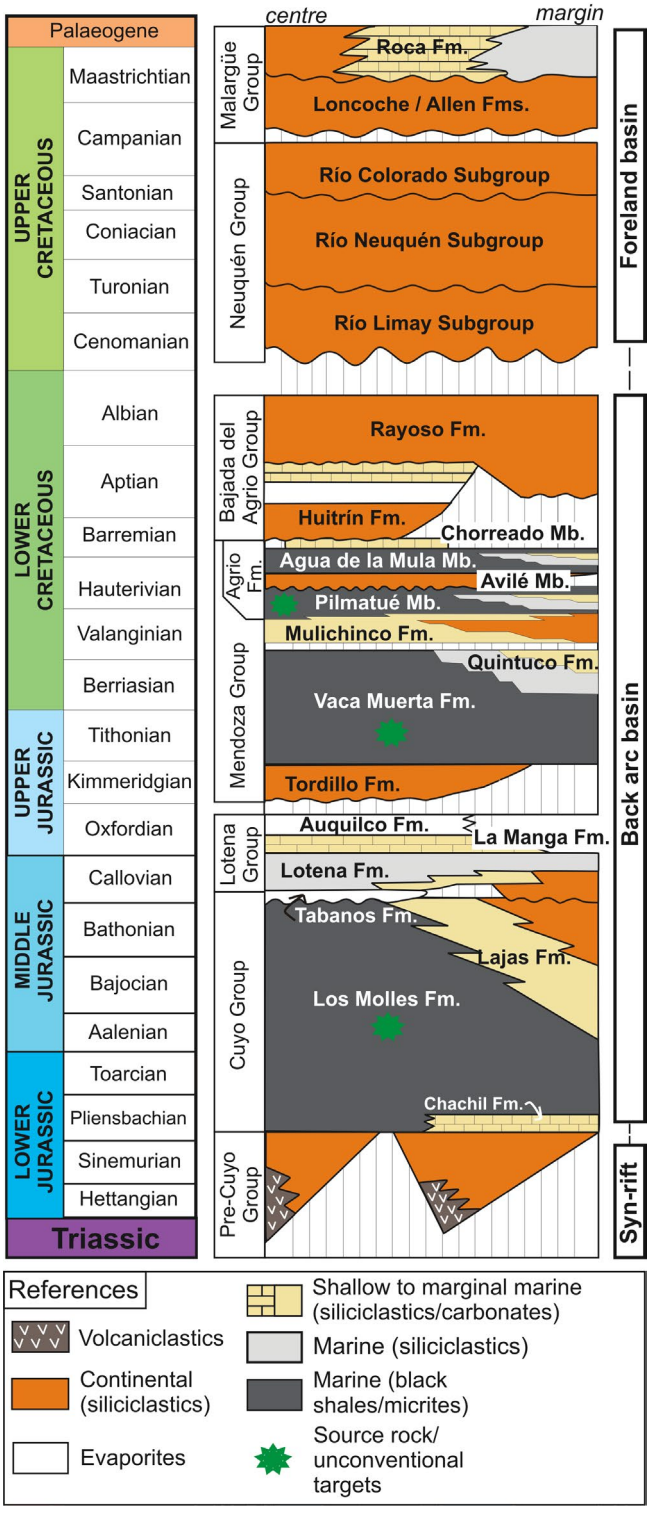

FIGURE 2 The classic stratigraphic chart for the Neuquén Basin (modified from Howell et al., 2005). The VMFm (Mendoza Group) represents the main source rock/unconventional target in the basin

of the Mendoza, Neuquén, Rio Negro and La Pampa provinces, Argentina (Howell et al., 2005; Vergani et al., 1995). Three stages of basin infill are summarized in Figure 2. The rift basin stage was characterized by several NW–SE rift depocentres formed during the Late Triassic–Early Jurassic with continental and volcanic deposits of the Precuyo Group (Franzese & Spalletti, 2001). A long thermal subsidence, interrupted by localized tectonic events, characterizes the retro-arc basin stage developed from the Early Jurassic to Early Cretaceous with thick marine and continental successions composed of carbonate, siliciclastic and evaporite facies (Howell et al., 2005; Legarreta & Uliana, 1991; Vergani et al., 1995). The lithostratigraphic framework includes the Cuyo, Lotena, Mendoza and Bajada del Agrio Groups (Groeber, 1946; Leanza, 2003; Stipanicic et al., 1968; Weaver, 1931), where marine organic-rich source rocks related to long-term Palaeo-Pacific transgressions are recorded: Los Molles, Vaca Muerta and Agrio Fms (Figure 2). Finally, the foreland basin stage in Late Cretaceous–Palaeocene time was linked to contractional conditions and associated with the Andean uplift (Horton, 2018). Sedimentation was dominated by synorogenic red bed successions (Neuquén Group) and the first shallow marine units (Malargüe Group) from the Atlantic Ocean (Aguirre-Urreta et al., 2011; Tunik et al., 2010). This stage was characterized by progressive growth of S–N fold and thrust belts (e.g. Agrio, Chos Malal and Malargüe) and reactivation of older extensional faults (Horton et al., 2016; Rojas Vera et al., 2015).

The VMFm, the focus of this study, represents a widespread marine transgression during the retro-arc stage, mainly composed of organic-rich black shales, marls and limestones reaching 800 m thickness (Legarreta & Uliana, 1991; Weaver, 1931). Based on ammonoid biozones, partially calibrated through high-precision U-Pb ages, the unit ranged from Tithonian–early Valanginian (e.g. Aguirre-Urreta et al., 2007; Naipauer et al., 2020; Vennari et al., 2014). Along the S–N fold and thrust belts, basinal-to-middle ramp deposits are well exposed and have been studied by detail facies analysis (e.g. Kietzmann et al., 2016; Otharán et al., 2020; Scasso et al., 2005; Spalletti et al., 2000). In the subsurface of the Neuquén Embayment, well logs, cores and seismic data provided additional information on the unit (e.g. Desjardins et al., 2016; Dominguez & Di Benedetto, 2019; Legarreta & Uliana, 1991; Mitchum & Uliana, 1985; Sagasti et al., 2014). Basin-scale stratigraphic architecture shows that the unit comprises three to five progradational sequences with organic-rich transgressive intervals composed of siliciclastic and carbonate-rich shales that grade upward into highstands dominated by organic-lean marls (Capelli et al., 2021; Dominguez et al., 2016; Kietzmann et al., 2016; Legarreta & Villar, 2015).

2.1 | Source rocks: An overview

Many studies have analysed the regional characteristics of the petroleum systems in the Neuquén Basin (Boll et al., 2014; Cruz et al., 1996, 2002; Karg & Littke, 2020; Kozlowski

et al., 1998; Legarreta et al., 2008; Mei et al., 2021; Rocha et al., 2018; Uliana & Legarreta, 1993; Vergani et al., 2011). The three marine source units are the Los Molles, Vaca Muerta and Agrio Fms, which differ in terms of organic richness, OM type, maturity and distribution throughout the basin. The oldest source rock was deposited during the Pleinsbachian–Callovian and covers, in the same way as the VMFm, almost the entire basin. The unit has present-day TOC ranging from 1% to 5% with kerogen types II (algal/amorphous macerals) and III (palynomorphs/phytoclasts macerals), showing a transition from immature to overmature stages (Jorgensen et al., 2013; Legarreta & Villar, 2011; Martínez et al., 2008). The thickness increases from approximately 500–900 m following the main NW–SE axis of the basin. However, important differences in thickness are related to inherited topography of the underlying rift depocenters (Legarreta & Villar, 2011; Olivera et al., 2020). Based on TOC contents, the lowermost part (ca. 200 m thick) shows the most suitable characteristics for a possible unconventional target (Jorgensen et al., 2013).

Based on organic geochemistry and petrological studies, the VMFm exhibits mainly amorphous (liptinitic macerals) type II kerogen with TOC content between 3% and 8% (peak values of 12%–20%) suitable for producing oil or gas condensate, depending on position in the basin (Brisson et al., 2020; Karg & Littke, 2020; Legarreta & Villar, 2011; Sylwan, 2014). The hydrocarbon yield expressed as original hydrogen index (HI_0) averages 680 mg_{HC}/g_{TOC} based on the analysis of immature samples (Brisson et al., 2020; Veiga et al., 2020). This is representative of the organic-rich intervals (30–450 m thick) considered to be the unconventional targets of the unit (Dominguez et al., 2016). Different patterns of organic richness, hydrocarbon source quality, distribution of free hydrocarbons and thermal maturity allowed Brisson et al. (2020) to distinguish six reference areas for the VMFm (Figure 1). Moderate depth of 3,000 m and overpressure conditions also make the unit a prime target for drilling operations and stimulation treatments which favour development and commercialization of this play (Badessich et al., 2016; Veiga et al., 2020).

The Agrio Fm includes two organic-rich intervals of late Valanginian and late Hauterivian age (e.g. Comerio et al., 2018; Pazos et al., 2020; Uliana & Legarreta, 1993). TOC content ranges from 1% to 5% with peak values of up to 16%, including type II and III kerogens (Comerio et al., 2018, 2020; Legarreta & Villar, 2012), with average measured HI_0 of 600 mg_{HC}/g_{TOC} for the type II intervals (Spacapan et al., 2018). Carbonate-rich shales are more enriched in type II kerogen than the siliciclastic shales, which are dominated by type III kerogen (Comerio et al., 2018). Maturity maps indicate that both intervals range in maturity from the oil window to the gas window (Cruz et al., 1996; Legarreta & Villar, 2012), reaching dry gas and overmature stages in areas where intrusions are present (Spacapan et al., 2018, 2020). Compared with VMFm, the Agrio Fm shows lower amounts of OM, lower effective thickness (<100 m thick), and reduced regional distribution.

3 | METHODOLOGY

The VMFm was analysed using a W–E section (Figure 1) along the Agrio fold and thrust belt (Agrio FTB). It includes information from 27 wells distributed throughout the section and available surface and seismic data. The present study shows organic geochemistry results and scanning electron microscopy images from cuttings and core samples from Well A (2,312–3,010 m), Well B (2,610–2,790 m) and Well C (2,270–2,430 m) on the Dorso de Los Chihuidos–NE Platform (Figure 1). We followed the stratigraphic scheme of Legarreta and Villar (2015) that subdivided the VMFm in lower, middle and upper VM to describe and interpret the results.

3.1 | Organic geochemistry

A total of 220 cuttings and core samples were analysed for present-day total organic carbon (TOC wt%) and Rock-Eval® programmed pyrolysis following standard procedures from the IFP Energies Nouvelles (Espitalié et al., 1986). Samples were solvent extracted to remove oil mud residues. The use of oil-based mud restricts the thorough evaluation of the unit because a quantitative measurement of free hydrocarbons (e.g. pyrolysis S1 peak, mg_{HC}/g_{ROCK}) is impossible, and many ratios used to interpret and evaluate the source beds cannot be employed in the analysis (Brisson et al., 2020). There are many equations used to calculate the original TOC (TOC_0) in source rocks (e.g. Brisson et al., 2020; Chen & Jiang, 2016; Modica & Lapierre, 2012; Peters et al., 2017). This study considers the equation specific for the VMFm, which was calculated based on an extensive pyrolysis data from cores and cutting samples from nearly 900 wells (see details in Brisson et al., 2020). These authors indicated a homogenous character of the type II kerogen and obtained an average of HI_0 of 680 mg_{HC}/g_{TOC} based on measures of immature samples (Brisson et al., 2020). The pyrolysis S2 (mg_{HC}/g_{ROCK}) and S3 (mg_{CO_2}/g_{TOC}) peaks allowed us to corroborate kerogen types and thermal maturity based on the T_{max} (Peters, 1986). Values of vitrinite reflectance (%Ro) were measured for Well A and Well B; however, for Well C (early oil window), the theoretical %Ro was calculated from T_{max} values (Brisson et al., 2020) due to the lack of vitrinite particles. The equation proposed by Brisson et al. (2020) is valid mainly for T_{max} between 410 and 470°C and was derived from a strong dataset. The usage of the equation in other source rocks should

be tested first due to the relationship between T_{max} and %Ro appears to be kerogen-type dependent (Katz & Lin, 2021). In addition, measured %Ro data from proximal wells and maturity maps were also considered to corroborate the maturity trend of Well C. Transformation ratio (TR) was calculated following the methodology of Waples and Tobey (2015), which expresses the converted mass fraction of the initial reactant, that is, the ratio of petroleum formed from kerogen in source rock to the total amount of petroleum that could be formed from that kerogen (Peters et al., 2017; Tissot & Welte, 1984).

3.2 | Scanning electron microscopy analysis

To examine microtextural features and evaluate the thermal transformation of OM, 22 core samples were prepared on thin sections normal to bedding planes, mechanically polished, ion-milled and analysed by field emission scanning electronic microscope (FE-SEM) at the Laboratorio de Analítica in YPF-Tecnología (Y-TEC) following internal procedures. Samples were coated with carbon and studied at different magnifications (from 150× to up to 200,000×) under secondary electron (SE) and backscattered diffraction (BSD) modes. Elemental composition of mineral phases was determined by energy-dispersive X-ray spectroscopy (EDS) microanalysis. Pore-size distribution was measured at different magnifications using the JMicrovision© (Roduit, 2008) program and considering OM pores as spherical to oval with bubble and spongy morphologies (Ko et al., 2017; Löhr et al., 2015; Milliken et al., 2013; Pommer & Milliken, 2015). FE-SEM resolution is in the order of 10 nm; and consequently, macropores (>50 nm) are well defined. However, part of the mesopores (2–50 nm) and micropores (<2 nm) are not measurable (pore sizes as defined by Rouquerol et al., 1994). Elongate pores with crack-like morphology were not considered because of possible generation during sample preparation (Katz & Arango, 2018; Löhr et al., 2015; Schieber, 2013).

4 | PETROLEUM SYSTEM MODELLING

Schlumberger 2-D PetroMod® software allows full integration of tectonic events, structural restoration, facies variation and source rock maturity through time. The software was used for sequential restoration of the Agrio regional cross section (Figures 1 and 3). To calibrate the BPSM and evaluate the history of hydrocarbon generation for the analysed source rocks, organic geochemistry and %Ro data from the VM, Los Molles and Agrio Fms were compiled (YPF database). The age, erosion thickness, lithologies, unit thickness and petroleum system elements for Well A and Well C are included in Supplementary Material 1.

4.1 | Modelling input

One-dimensional (1-D) and 2D BPSMs were performed using PetroMod® Teclink® software (Hantschel & Kauerauf, 2009), including coupled structural restoration and backstripping tools. This technique integrates the structural and the petroleum systems model, which is essential for simulating hydrocarbon generation, migration and accumulation in tectonically complex areas. Software calculations in tectonically complex areas are analysed in detail by Hantschel and Kauerauf (2009) and Burgreen-Chan et al. (2015). PetroMod® software provides a database to estimate the surface–water interface temperature (SWIT). The upper boundary condition for temperature calculations is determined by the sediment–water surface (onshore) temperatures (Hantschel & Kauerauf, 2009; Peters et al., 2017). In the model, SWIT data were corrected for present and past water depth (Supplementary Material 2). It uses a global reconstruction of the palaeo-mean surface or air temperatures and palaeobathymetry to estimate SWIT for a given latitude (Wygrala, 1989). The most important input for predicting hydrocarbon generation is the evolution of thermal heat flow through geologic time, which together with the burial history, controls the evolution of temperature and chemical reactions during the generation, migration, accumulation and preservation of petroleum. Thermal history of the Agrio section was reconstructed assuming a constant heat flow of 60 mW/m^2 through time (Supplementary Material 2). Heat flow was calibrated with %Ro data and later cross-checked with Horner-corrected bottom-hole temperature (Deming, 1989). Similar constant heat flow of 60 mW/m^2 was assumed by Lampe et al. (2006) for the Agrio FTB. The resulting temperature fields provided theoretical values for temperature, %Ro, TOC, Øorg and TR, and were used to calculate the amount of cracked kerogen. Source rock maturation assessed using the Easy %Ro equation from Sweeney and Burnham (1990). Lithological properties were based on Athy's compaction law (Athy, 1930) and the multipoint model (Hantschel & Kauerauf, 2009). Athy's law is a traditional porosity versus depth curve which predicts hydrostatic pressure based on deposition of the entire column with various lithologies. Additionally, the PetroMod® software allowed to simulate effective and secondary porosity. Effective porosity is the pore volume in a rock that contributes to the permeability and does not include isolated vuggy porosity or water that is bound to clay minerals (Hantschel & Kauerauf, 2009). Secondary porosity in a source rock is the additional porosity that can be generated by mineral transformations (inorganic secondary porosity) or transformation of OM into hydrocarbons (organic secondary porosity). PetroMod® software calculates the Øorg as the cumulative amount of porosity generated during OM transformation.

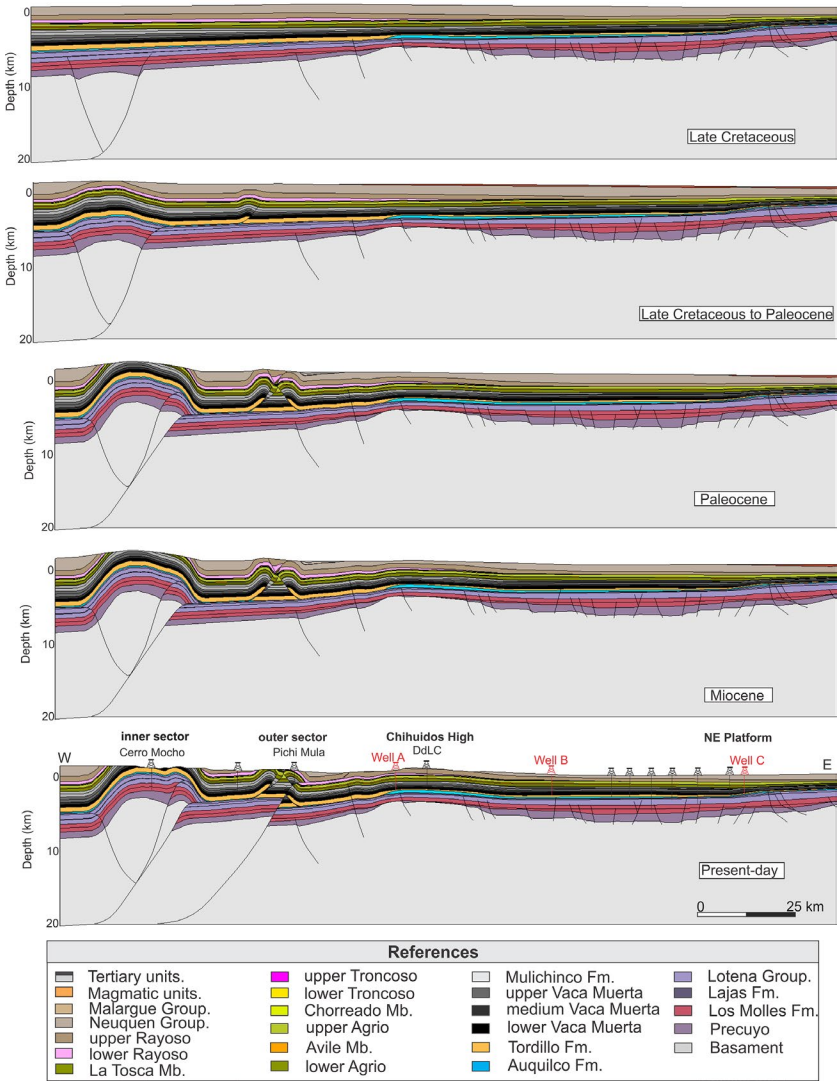

FIGURE 3 Tectonic evolution for the Agrio FTB cross section from the Late Cretaceous to present day (see also Rocha et al., 2018)

In addition, it predicts the proportion of gas adsorbed within OM pores or on mineral surfaces versus free gas in pore spaces or natural fractures (Peters et al., 2017). Furthermore, the evolution of Øorg and its relationship with the burial history were analysed through the effective porosity curve. Pore pressure prediction is important for executing a safe drilling strategy and for accurate production modelling (Couzens-Schultz et al., 2013). Fluid pressure modelling can be used to improve pore pressure prediction and reduce the drilling risk posed by unanticipated overpressures (Peters et al., 2017). Diagnostic fracture injection testing (DFIT) data obtained from the YPF database were used to calibrate pressure conditions in the analysed wells.

4.2 | The Agrio Fold and Thrust Belt (FTB): Balanced structural section

The Agrio FTB extends from the 38°50′ to 37°35′ S and is characterized by two sectors with different structural styles (Vergani et al., 1995; Zamora Valcarce et al., 2007; Zapata & Folguera, 2005). To the west, the inner sector shows basement deformation and tectonic inversion of previous extensional (Triassic) structures (Ramos et al., 2011; Rojas Vera et al., 2010). The outer sector is dominated by thin-skinned deformation showing basal detachments within Jurassic and Lower Cretaceous evaporites and marine shales with a general deformation sense to the east and several west-verging backthrusts (Rojas Vera et al., 2015; Zamora Valcarce et al., 2011). To the east, the Dorso de Los Chihuidos (DdLC) is defined by an antiformal structure interpreted as the result of tectonic inversion of basement involved normal faults (Ramos et al., 2011). Such differences control the distribution of outcrops in the central part of the Neuquén Basin with Jurassic sedimentary units (Cuyo and Lotena Groups) mainly exposed in the inner sector and Upper Jurassic–Cretaceous units (Mendoza, Bajada del Agrio and Neuquén Groups) to the east in the outer sector (Leanza & Hugo, 2001; Rojas Vera et al., 2015; Zamora Valcarce et al., 2007, 2011). Balanced structural section published by Rocha et al. (2018) was used in this study, which extends from the Agrio FTB (inner and outer

sectors), the DdlC (Well A), external flank of the DdLC (Well B) to the NE Platform (Well C) (see location in Figures 1 and 3). This section was sequentially restored with the aim to represent the tectonical evolution based on available information. Initial exhumation occurred in the Late Cretaceous (Rojas Vera et al., 2015; Tunik et al., 2010), with two peaks of reactivation in the Oligocene–Miocene and middle Miocene based on apatite fission tracks (Rocha et al., 2018). The Agrio FTB represents the most important depocentre during the Mesozoic sedimentation and includes the embayment sector where the VMFm reached highest maturity (Brisson et al., 2020). The Mesozoic succession thins northward in the domain of Chos Malal FTB, a sector known as Chihuido–Lomita as well as to the basin margin (NE platform) characterized by shallower burial and lower maturity levels.

5 | RESULTS

5.1 | Vaca Muerta organic geochemistry

The results from programmed pyrolysis are summarized in Table 1. The TOC content in all analysed wells is high with mean values that range from 2.38% (Well A), 5% (Well B), to 3.21% (Well C) in the Agrio section (Figure 4). The lower and middle VM contain the highest TOC contents, with highest values towards basinal (west) settings: 3.60% and 3.76% (Well A), 8% and 4.83% (Well B) and 3.36% and 3.05% (Well C).

Well C shows Rock Eval® T_{max} values that range from 429 to 443°C (mean: 435°C) and calculated %Ro between 0.65 and 0.90 (mean value: 0.80), which is consistent with the early oil window (Figure 5a). %Ro measures indicate a range from 1.60–1.65 (wet gas, Well B) to 2.10–2.33 (dry gas, Well A) (Figure 4). The S2 peak that coincides with the remaining potential of hydrocarbon generation decreases towards high-maturity zones ranging from 15.44 mg_{HC}/g_{ROCK} (1.34–43.15 minimum and maximum values) in the early oil (Well C) to 0.68 mg_{HC}/g_{ROCK} (0.21–1.49) in the dry gas zone (Well A). On the contrary, T_{max} displays increased thermal maturity, reaching mean values of 475°C (460–514°C minimum and maximum values) in the wet gas window (Well B). T_{max} cannot be measured in the dry gas window (Well A) due to very low values of S2 indicating that hydrocarbon-generative capacity of the OM has been exhausted.

The mean values of HI also decrease as maturity increases from 470 mg_{HC}/g_{TOC} (238–654 minimum and maximum values) in the early oil (Well C) to 41 mg_{HC}/g_{TOC} (6–107) in the dry gas window (Well A) for the Agrio section (Table 1). The oil-prone VMFm throughout the basin is supported by the presence of bacterial/algae OM (Brisson et al., 2020; Petersen et al., 2020) and is consistent with low values of oxygen index (OI) in all analysed wells (mean values between 8 and 47 mg_{CO_2}/g_{TOC}). However, the uppermost levels of the upper VM at Well A record an increase in OI (Figure 4). The pseudo-van Krevelen diagram (hydrogen vs. oxygen index, Figure 5b) shows that most samples lie close to the HI-axis and reflect increasing maturity of the analysed wells with HI depletion from the early oil to dry gas windows. This explains the type II kerogen identified in samples from the early-to-peak oil window. More mature samples in the wet and dry gas windows plot near the origin of the diagram.

The transformation ratio ($TR = [HI_0 - HI_{sample}]/HI_0 \times 100\%$, sensu Waples & Tobey, 2015) increases with maturity, showing mean values from 30% (3%–64%) at Well C, 97% (94%–98%) at Well B to 93% (84%–99%) at Well A. The equation presented by Brisson et al. (2020) was used to restore the original total organic carbon TOC_0 content (Table 1). For the lower VM, average TOC_0 contents range from: 8.24% (1.10%–15.50%) at Well A, 18.60% (7.29–27.41) at Well B to 6.86% (0.56–14.35) at Well C (Table 1).

5.2 | OM and its related pores under SEM

5.2.1 | Oil window

Well C samples correspond to the early oil window and with respect to OM two forms are documented (Figure 6). Some samples exhibit filament-like OM that defines a discontinuous wavy-parallel lamination that is disposed between silt-size detrital grains, calcareous debris and faecal pellets mainly composed of calcareous coccoliths (Figure 6a–c). These OM domains likely represent relicts of marine type II kerogen compressed by mechanical compaction between rigid detrital grains. In such levels, the OM does not show evidence of pores at SEM resolution. Conversely, other samples show OM that is intimately bound to the inorganic matrix composed of coccolith debris, illite/mica phyllosilicates and quartz, plagioclase and carbonate fragments (Figure 6d,e). The OM mostly fills intergranular pore space and lacks the filament-like structure. It occupies the interstices between those detrital components and within primary pores such as those related to pressure shadows (Schieber, 2010), and it fills microfossil-related voids (Figure 6f). Isolated, bubble pores of variable size (40–1,000 nm, mean 200 nm) are documented. OM of detrital (terrigenous) origin occurs in few samples and in minor amounts, which is consistent with little land-derived OM in the VMFm (Brisson et al., 2020; Małachowska et al., 2019; Petersen et al., 2020). Nonporous OM of terrigenous origin (e.g. vitrinite and inertinite) is present as rigid grains with discrete arcuate margins (Milliken et al., 2013; Pommer & Milliken, 2015). Phyllosilicate framework pores with triangular to elongated geometries (200–1,400 nm wide) are less common. Microfractures (6–15 μm thick by more than 600 μm in length, Figure 6f) oriented subparallel to bedding planes and partially filled with secondary products (solid bitumen) are also documented.

TABLE 1 Summary with organic geochemistry results for the lower, middle and upper informal units of the Vaca Muerta Formation in the Agrio section (general includes all samples of the well)

	Vaca Muerta units	TOC %	S1 mg/g	S2 mg/g	S3 mg/g	T_{max} °C	HI = S2/TOC mg/g	OI = S3/TOC mg/g	TR = HI_0 − HI/HI_0 % Waples and Tobey (2015)	TOC_0 % Brisson et al. (2020)
Well C (early oil)	Middle	3.05 (0.44–7.99)	0.15 (0.11–0.35)	15.62 (1.34–43.15)	0.52 (0.28–1.06)	434 (429–441)	497 (255–654)	25 (4–120)	26 (3–62)	6.06 (0.42–17.49)
	Lower	3.36 (0.57–6.39)	0.23 (0.06–0.91)	15.28 (2.16–40.18)	0.48 (0.19–0.87)	437 (429–443)	448 (238–628)	17 (5–45)	34 (7–64)	6.86 (0.56–14.35)
	General	3.21 (0.44–7.99)	0.19 (0.06–0.91)	15.44 (1.34–43.15)	0.50 (0.19–1.06)	435 (429–443)	470 (238–654)	21 (4–120)	30 (3–64)	6.49 (0.42–17.49)
Well B (wet gas)	Upper	3.33 (0.40–7.44)	0.10 (0.06–0.16)	0.63 (0.13–1.66)	0.27 (0.21–0.50)	480 (460–512)	21 (12–38)	13 (4–56)	96 (94–98)	7.63 (0.87–17.11)
	Middle	4.83 (2.36–7.10)	0.10 (0.07–0.16)	0.81 (0.43–1.26)	0.28 (0.22–0.34)	466 (460–476)	17 (12–20)	6 (4–11)	97 (97–98)	11.21 (5.41–15.90)
	Lower	8 (3.18–12)	0.10 (0.07–0.15)	1.37 (0.52–2.67)	0.26 (0.17–0.33)	477 (466–514)	17 (13–24)	4 (2–7)	97 (96–98)	18.60 (7.29–27.41)
	General	5 (0.40–12)	0.10 (0.06–0.16)	0.87 (0.13–2.67)	0.27 (0.17–0.50)	475 (460–514)	18 (12–38)	8 (2–56)	97 (94–98)	11.50 (0.87–27.41)
Well A (dry gas)	Upper	1.75 (0.46–4.50)	0.19 (0.10–0.39)	0.71 (0.21–1.49)	0.76 (0.45–2.31)	Unmeasurable T_{max}	51 (6–107)	59 (11–142)	92 (84–99)	3.92 (0.97–11.38)
	Middle	3.76 (1.47–5.0)	0.27 (0.16–0.50)	0.61 (0.35–0.84)	0.76 (0.53–1.10)		17 (11–28)	23 (11–47)	97 (95–98)	8.62 (3.32–11.20)
	Lower	3.60 (0.50–6.74)	0.23 (0.10–0.36)	0.60 (0.26–0.91)	0.58 (0.32–0.80)		28 (11–60)	28 (11–72)	95 (91–98)	8.24 (1.10–15.50)
	General	2.38 (0.46–6.74)	0.21 (0.10–0.50)	0.68 (0.21–1.49)	0.74 (0.32–2.31)		41 (6–107)	47 (11–142)	93 (84–99)	5.40 (0.97–15.50)

Note: Minimum, maximum and mean values are presented.

Abbreviations: HI, hydrogen index; HI_0, original hydrogen index; OI, oxygen index; S1, S2 and S3, peaks derived from the programed pyrolysis; T_{max}, temperature reached in the S2 peak; TOC, total organic carbon; TOC_0, restoration of original TOC; TR, transformation ratio.

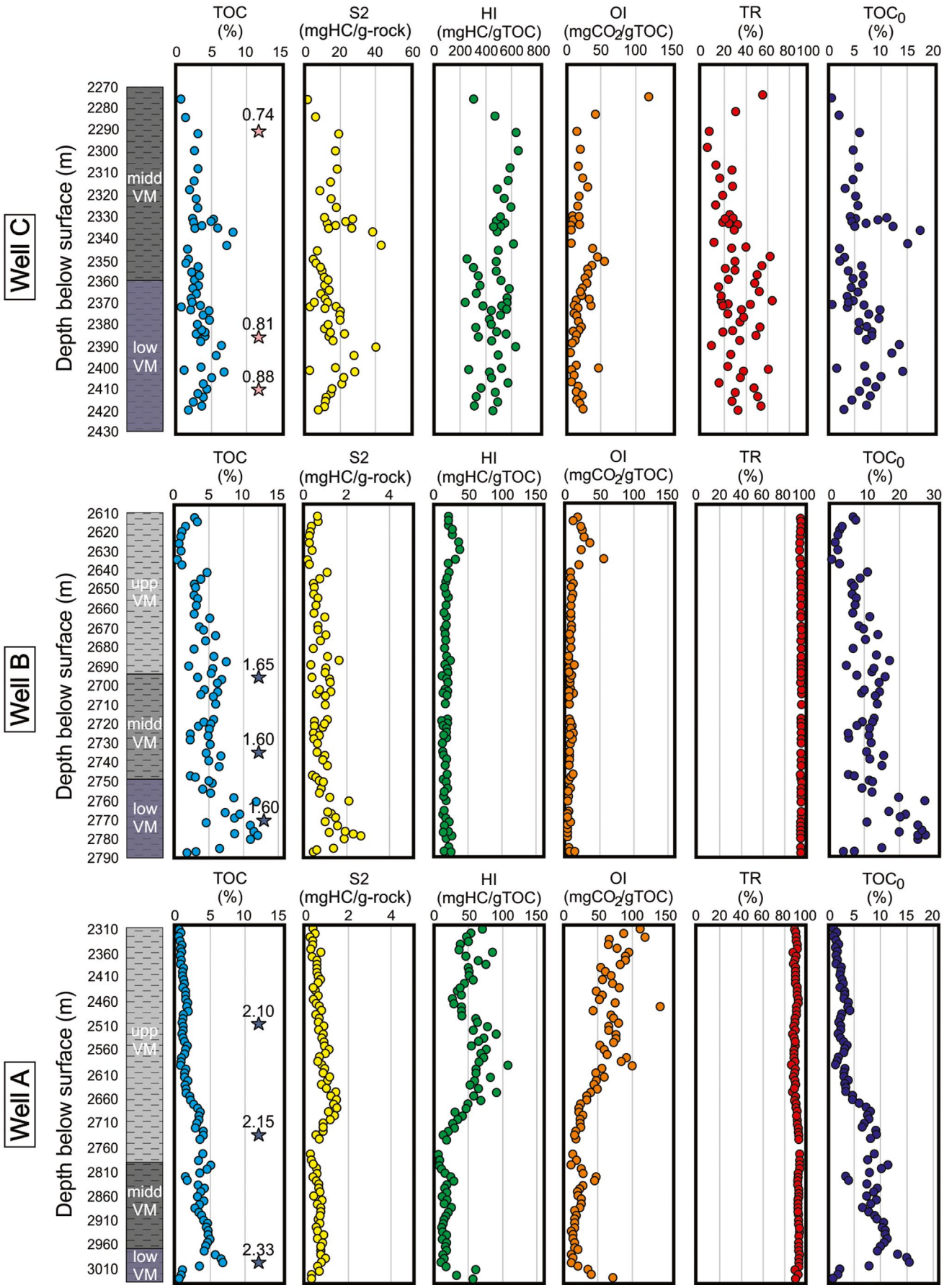
Well C
Well B
Well A
Depth below surface (m)
TOC (%)
S2 (mgHC/g-rock)
HI (mgHC/gTOC)
OI (mgCO2/gTOC)
TR (%)
TOC0 (%)
midd VM
low VM
upp VM
0.74
0.81
0.88
1.65
1.60
1.60
2.10
2.15
2.33

FIGURE 4 Organic geochemical logs for the analysed wells in the Agrio section. Blue stars (Wells A and B) represent vitrinite reflectance (%Ro) values and pink stars (Well C) are theoretical %Ro values based on Brisson et al. (2020). TR and TOC_0 were calculated following the methodology of Waples and Tobey (2015) and Brisson et al. (2020)

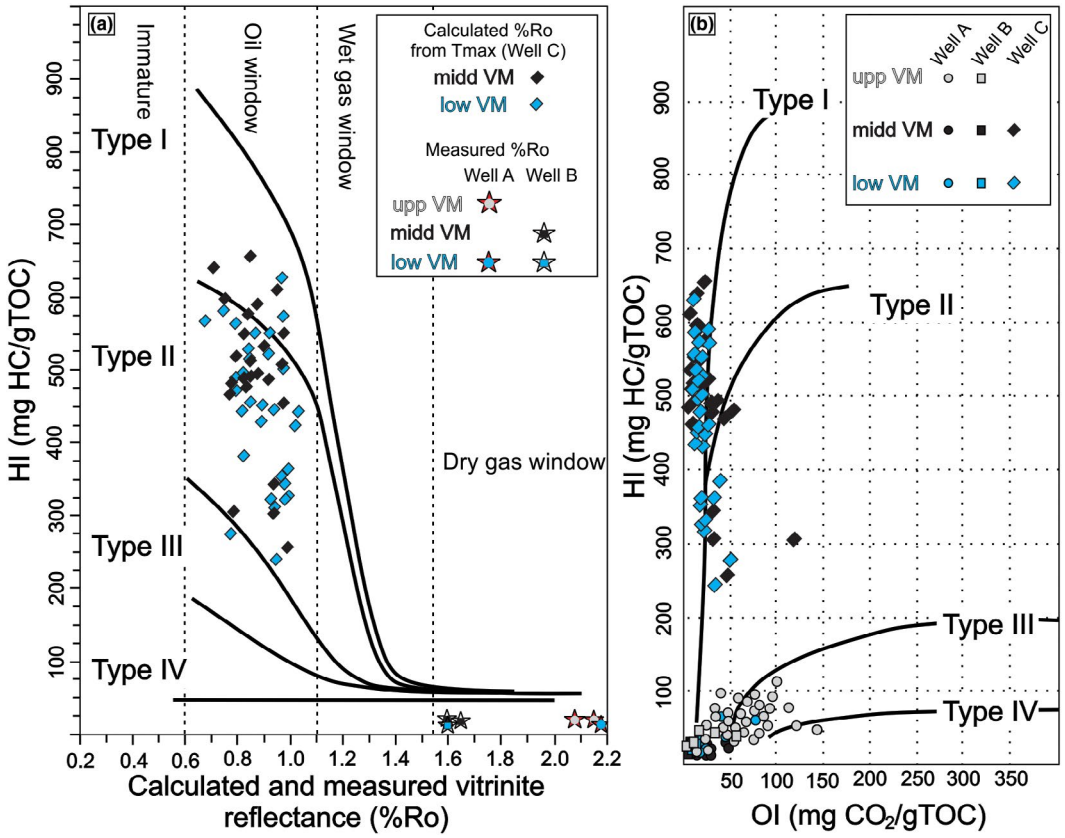

FIGURE 5 Organic geochemical results for the lower, middle and upper VM (informal stratigraphic units defined by Legarreta & Villar, 2015) in the analysed wells along the Agrio (Well A, Well B and Well C) sections. (a) Hydrogen index (HI) versus calculated and measured %Ro values. Calculated %Ro based on the equation of Brisson et al. (2020) for Well C (early oil window). Measured %Ro values are given for Well A and Well B (gas window) and indicated with star markers. (b) HI versus oxygen index (OI) based on the pseudo-van Krevelen diagram

5.2.2 | Gas window

Samples of gas window maturity are dominated by OM of secondary origin (see Mastalerz et al., 2018; Pommer & Milliken, 2015), which were identified as solid bitumen, the dominant organic component in thermally mature samples of the VMFm (Cavelan et al., 2019; Petersen et al., 2020; Romero-Sarmiento et al., 2017). As mentioned previously, OM is associated with the mineral matrix (intergranular space) and fills cavities within bioclasts and fractures (Figures 7 and 8). Compared with the oil window, however, samples from the gas window show a larger range of pore sizes. Wet gas samples (Well B) record large (2–4 μm) OM-hosted bubble pores protected by rigid mineral phases as well as calcite bioclasts (Figure 7a–c). Nevertheless, some elongated bubble pores suggest that compaction impacted OM pores (Figure 7e). OM pervasively fills intergranular spaces and contains both spongy and bubble pores (Figure 7d–f), which is typical of the gas window (Ko et al., 2017). Equivalent samples from the gas window in the VMFm analysed by Cavelan et al. (2019) also show secondary solid bitumen with bubble and spongy morphologies. In the present study, SEM reveals that bubble and spongy morphologies co-exist (Figure 7d–f), between diameters of 4 μm–800 nm (mean 500 nm) and 10–90 nm (mean 55 nm), respectively.

Samples from the dry gas window (Well A) also show secondary OM products (solid bitumen) with spongy and bubble pores (Figure 8a–d). However, very small and widely distributed spongy pores dominate (Figure 8e,f). The OM is confined within matrix cavities and is associated with both detrital and authigenic clays as well as microcrystalline quartz and calcite cement (Figure 8b–e). In the case of the VMFm,

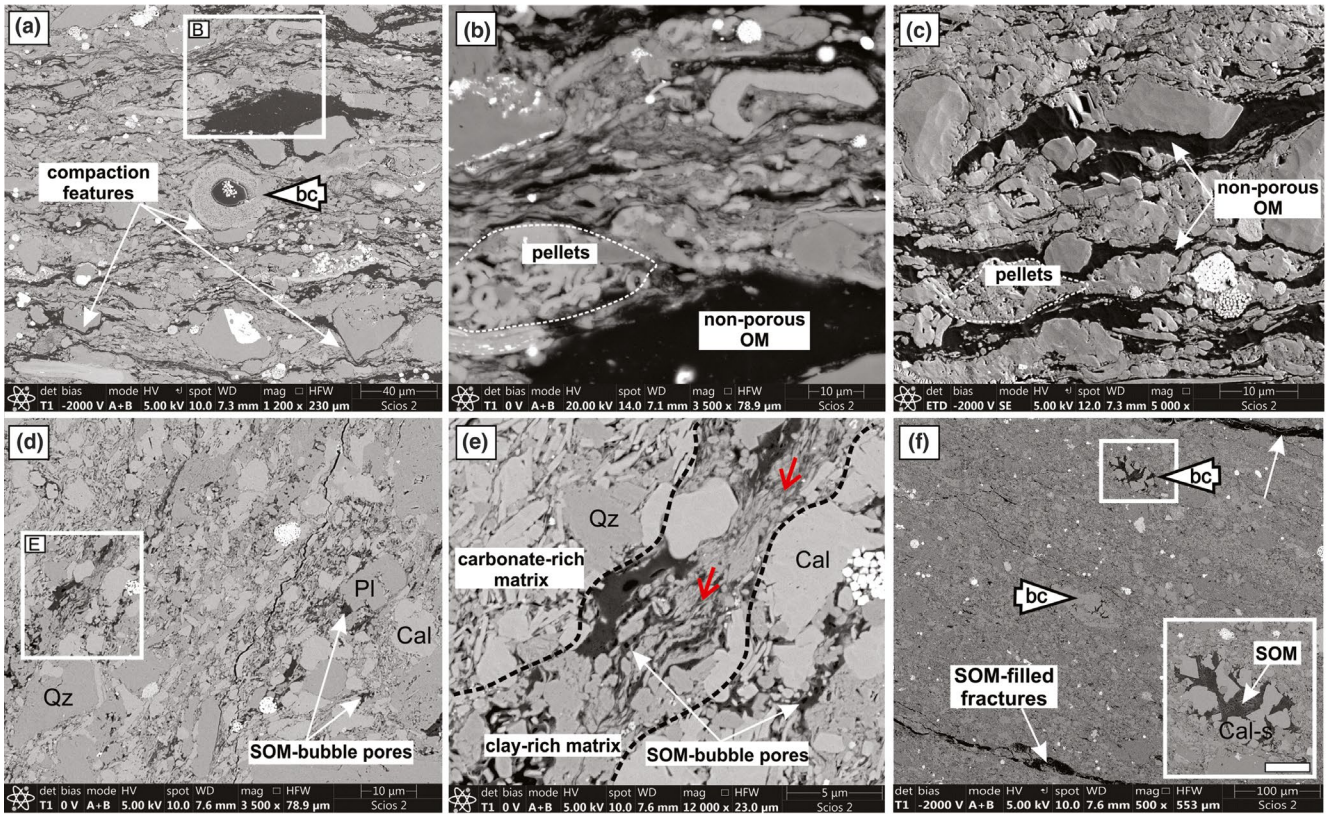

FIGURE 6 SEM images of low-maturity samples (Well C). (a–c) Examples of nonporous organic matter (OM) (marine type II kerogen in the VMFm). Note compactional features among rigid detrital grains, which in some cases are enclosed by a thin envelope of OM. Faecal pellets composed of coccoliths and bioclasts (bc) filled with OM. (d, e) General and detail with the secondary organic matter (SOM) that hosts isolated bubble pores. OM is distributed between detrital grains: Qz (quartz), illite/mica (red arrows) and carbonates (Cal). (f) SOM-filling microfractures and bioclasts (bc) associated with spar calcite (Cal-s). The insert shows a detail image (scale bar = 20 μm)

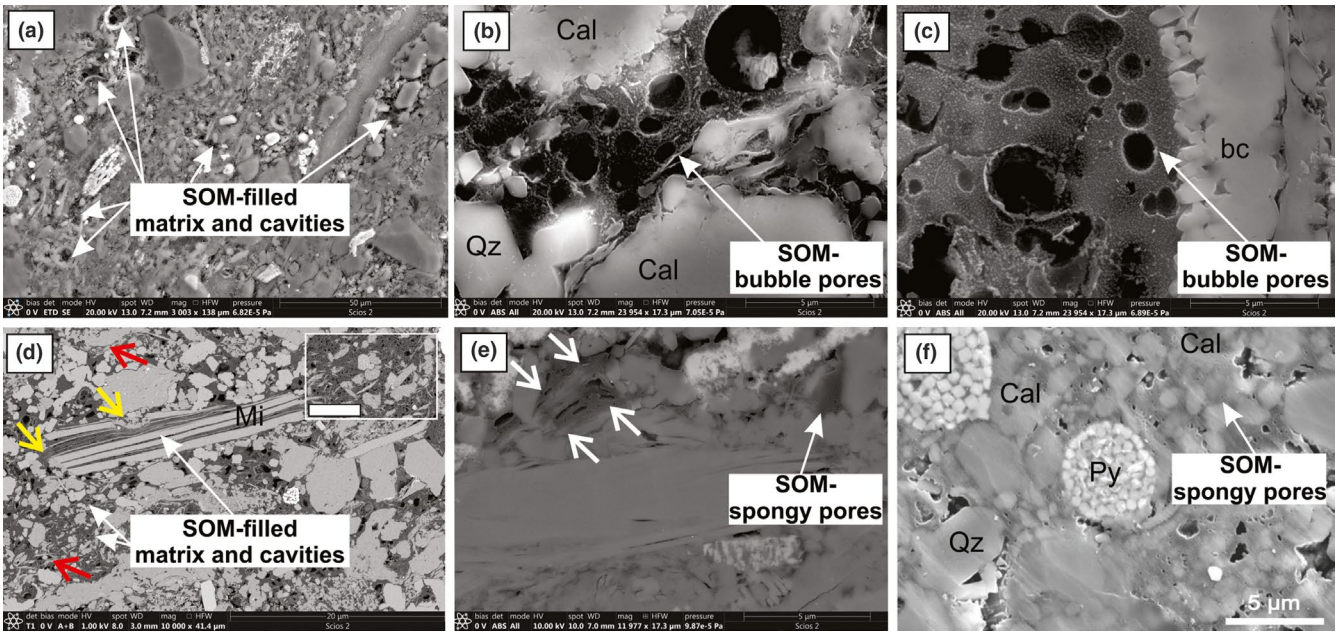

FIGURE 7 SEM images of wet gas window samples (Well B). General (a) and detailed images (b, c) showing secondary organic matter (SOM) filling matrix pores and bioclasts. The excellent preservation of bubble pores is linked with quartz (Qz) and calcite (Cal) cements and calcite bioclasts (bc). (d) SOM shows both bubble and spongy pores. Note expanded mica (Mi), detrital (red arrows) and authigenic (yellow arrow) illite. The insert shows detail of spongy pores (scale bar = 2 μm). (e) Elongate bubble pores (white arrows). (f) SOM-hosted spongy pores among diagenetic microcrystalline quartz (Qz), pyrite framboids (Py) and calcite (Cal)

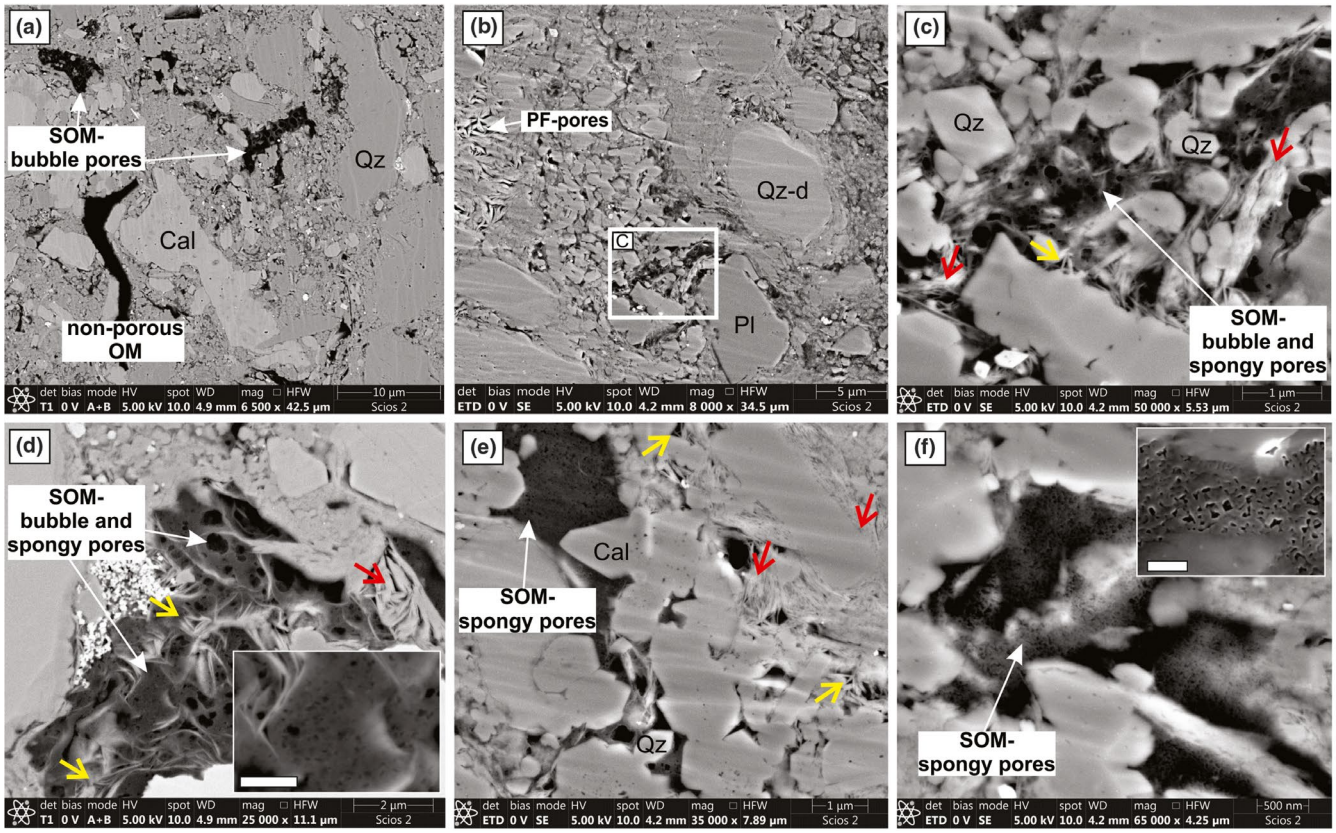

FIGURE 8 SEM images of dry gas window samples (Well A). (a) Secondary organic matter (SOM)-hosted bubble pores and nonporous terrigenous OM. (b, c) General and detailed images with SOM-filling pores between detrital (Pl = plagioclase; Qz-d = quartz) and diagenetic quartz. Phyllosilicate pores (PF-pores) are also documented. In (c) note diagenetic quartz (Qz) and illite of detrital (red arrows) and diagenetic (yellow arrow) origin. (d) SOM with bubble and spongy pores. The OM is associated with clay minerals of both detrital (red arrow) and diagenetic (yellow arrows) origins. The insert shows spongy pores (scale bar = 500 nm). (e) SOM with spongy pores filling a cavity partially cemented by calcite (Cal) and microcrystalline diagenetic quartz (Qz). There are illite/mica domains of detrital origin (red arrows) and authigenic crystals (yellow arrows) that grew from detrital crystals. (f) Spongy pores. Note detail in the insert image (scale bar = 200 nm)

siliceous and calcareous biogenic components are interpreted to contribute to the precipitation of microquartz and calcite (Milliken et al., 2019). There is also nonporous, elongate OM interpreted of terrigenous origin (Figure 8a). Pores associated with the phyllosilicate framework are represented by triangular-shaped openings (70–1,200 nm wide, Figure 8b) as was documented in overmature samples of the Middle Devonian Geneseo Fm (Northern Appalachian Basin) by Wilson and Schieber (2016). In the case of OM-hosted pores, samples of the VMFm that experienced high-thermal maturity range in size from 15 to 80 nm (mean 40 nm) for the spongy and 100 to 700 nm (mean 200 nm) for the bubble pores.

6 | BASIN AND PETROLEUM SYSTEM MODELLING (BPSM)

The quantification of source rock maturity, hydrocarbon generation and expulsion, pore pressure distribution and porosity (primary and secondary) was analysed in the regional 2-D BPSM (Agrio section). BPSM fully integrated the main rock parameters, such as kerogen type, TOC_0, Øorg, TR, maturity (%Ro) and tectonic events. The 2D modelling was conducted for the three effective source rocks in the basin (Los Molles, Vaca Muerta and Agrio Fms). In particular, this study presents data used to calibrate those parameters in the VMFm because the study focuses on characterization of processes within this unit through geological time.

6.1 | Well calibration in the Agrio model

The conditions of temperature, OM content, maturity, porosity and pore pressure were calibrated using a robust data set from wells along the Agrio section (Figures 3 and 9). Data presented correspond to Well A (DdLC) and Well C (NE Platform), which represent different geological scenarios, because they are located in different basin regions (see

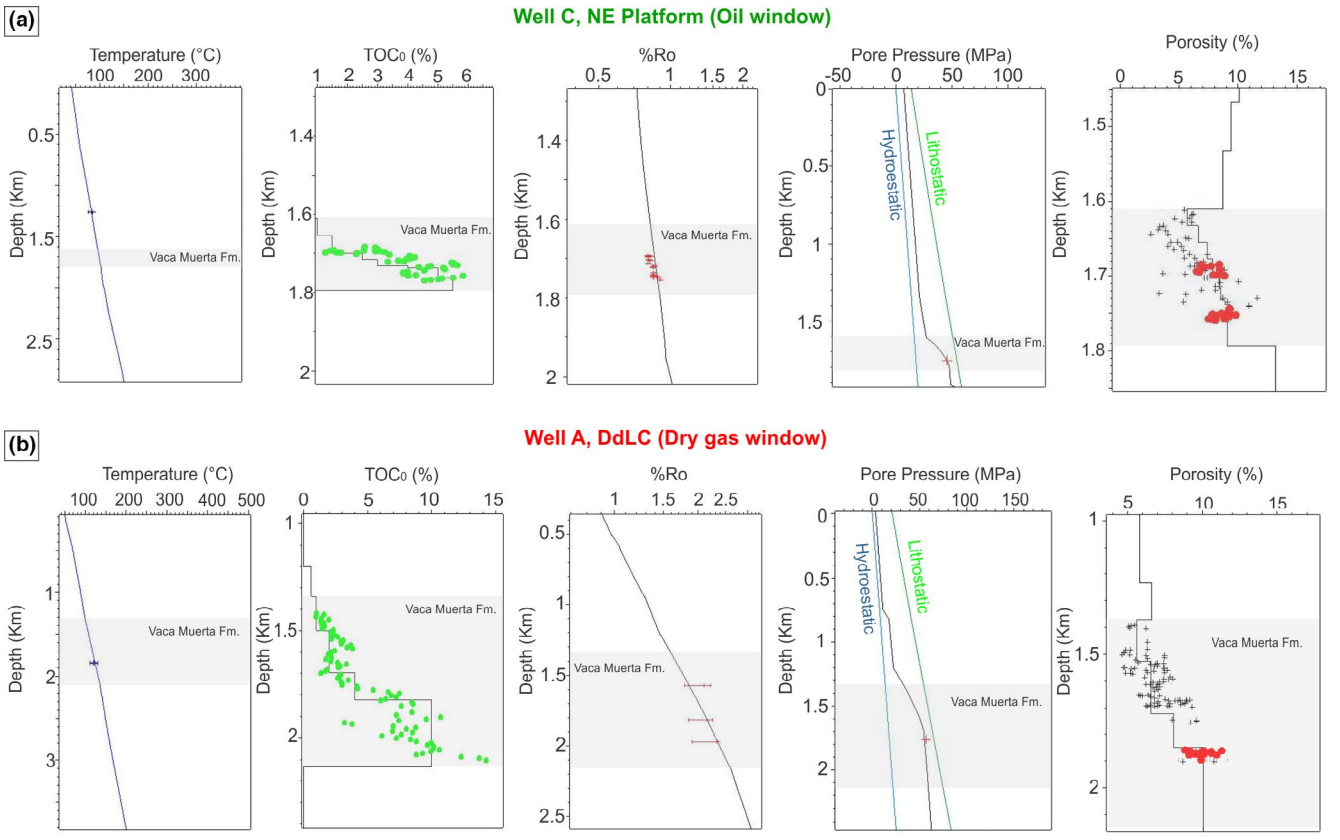

FIGURE 9 Well calibration of different parameters in the Agrio section for Well C (NE Platform) in (a) and Well A (DdLC) in (b). From left to right: calculated temperature log (blue line). Black markers are Hornet-corrected borehole temperatures. TOC_0 log showing the simulated organic matter concentration (black curve). Green circles represent TOC_0 values obtained from present-day TOC contents. Vitrinite log calculated with the equation of Sweeney and Burnham (1990) Easy %Ro kinetic algorithm. %Ro vitrinite values (red markers) were used to calibrate the calculated %Ro curve (black curve). Vertical profile showing the calculated pore pressure magnitude (black line), red crosses are the pore pressure determined from DFIT tests. Calculated porosity (black curve) was calibrated using measures obtained from well logging (black cross) and gas-filled porosity (red markers) from core samples. Depth is expressed in depth subsea

Figure 3). The thermal evolution of the model was calibrated using Horner-corrected borehole temperature data (BHT), whereas the TOC_0 was calculated from pyrolysis data and used to adjust the evolution of TOC_0 for the lower, middle and upper VM in the model (Figure 9). Model and pyrolysis results show an increase in the TOC_0 content from the top to the base of the unit. %Ro measures were used to calibrate the thermal maturity, which indicates that the VMFm reached the dry gas window (Well A, western flank of the Chihuidos High) and the early oil window (Well C, NE Platform). In order to calibrate pore pressure, we use data from DFIT. DFIT is used as an indirect method to estimate pore pressure in unconventional reservoirs (Bakar, 2018). According to DFIT data (red crosses in Figure 9), overpressure increases towards the foreland (west) region. A high pore pressure of ca. 57 MPa is registered at ca. 2,600 m depth in Well A and it is close to the lithostatic pressure, as was also documented by Berthelon et al. (2021). Well C has a pore pressure of ca. 48 MPa at ca. 2,200 m depth. The effective porosity was calibrated by using both well log (black crosses in Figure 9) and gas-filled porosity (red dots in Figure 9) data (YPF database). Results are consistent with previous studies (Askenazi et al., 2013; Cuervo et al., 2016; Ortiz et al., 2020) and show that the effective porosity increases towards the lower VM (Figure 9). In Well A, this parameter ranges from 5.5% to 12.16% (9.1% average), whereas in Well C effective porosity ranges from 3.24% to 8.44% (6.25% average).

6.2 | Hydrocarbon generation in the Agrio model

Evolution of the TR through time for the VMFm was compared with the Los Molles and Agrio Fms and analysed in four stages of sequential restoration (Figure 10). During the Late Cretaceous (ca. 100 Ma), TR of 95% suggests that organic-rich deposits of the Los Molles Fm in the inner sector reached the advanced dry gas window (Figure 10a). From the inner sector to the eastern flank of the DdLC, the lower VM would have reached a TR average value of 95%. Expulsion

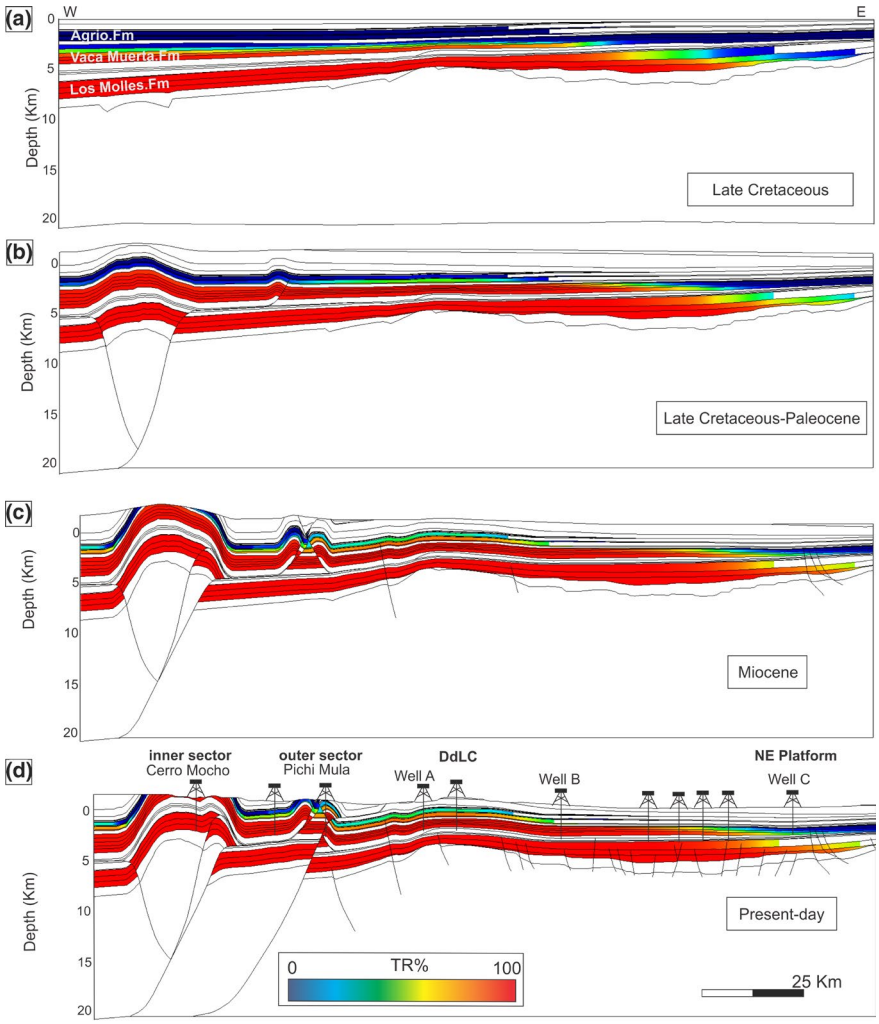

FIGURE 10 Modelling of thermal maturity based on transformation ratio (TR%) in the Agrio cross section for the three source rocks in the basin. Four stages of sequential restoration are considered. (a) Late Cretaceous, (b) Palaeocene, (c) middle Miocene and (d) present day

started during the Early Cretaceous (ca. 130 Ma) at a thermal maturity of 0.82–0.90 %Ro. Likewise, the western organic-rich deposits of the Agrio Fm reached the early oil window, with a TR of 15% approximately (Figure 10a). The model predicts that large volumes of hydrocarbons were generated and expelled from the Los Molles Fm and lower VM. Such processes were synchronous with the deposition of the Bajada del Agrio Group and before the formation of the main tectonic structures in the inner sector of the belt. A marked thickness increase in the Los Molles and VMFms was predicted in western areas where the beginning of hydrocarbon generation took place between the Late Jurassic and Early Cretaceous. From 90 to 60 Ma, more than 1,000 m of sediments were deposited (Neuquén and Malargüe Groups), which exhausted the generation capacity of the Los Molles and VMFms from the inner sector to the DdLC. These results suggest that gas generation related to secondary cracking reactions was a relevant factor in the early development of overpressure in the VMFm.

The first compressional tectonic event started between 70 and 60 Ma (Late Cretaceous–Palaeocene) and triggered basement fault inversion in the Agrio FTB and uplifting of the Cerro Mocho anticline in the inner (west) sector (Figure 10b). Shortening between the inner and outer sectors was accommodated through a basal detachment in the Auquilco evaporites. During this stage, the western organic-rich deposits of Los Molles Fm and lower VM were thermally overmature, whereas the kitchen of Agrio Fm would have reached a 45% transformation (Figure 10b). To the NE platform, the base of the VMFm would have reached more than 30% transformation (Figure 10b).

During the middle Miocene (14 Ma), the model predicts that kerogens of the Los Molles Fm and lower VM were fully transformed in the inner and outer sectors of the belt (Figure 10c). In those areas, the Los Molles source rock reached the advanced dry gas window to overmature (>4 %Ro). The VMFm source rock was in the gas window, whereas the Agrio Fm reached an average TR of 85% (Figure 10c). Miocene compression resulted in uplift of the inner sector and the structural duplication of sedimentary successions in the outer sector. The Miocene deformation phase promoted uplift and cooling of the main source rocks in the inner sector. Tectonic uplift temporally stopped thermal maturation and secondary cracking, in conjunction with

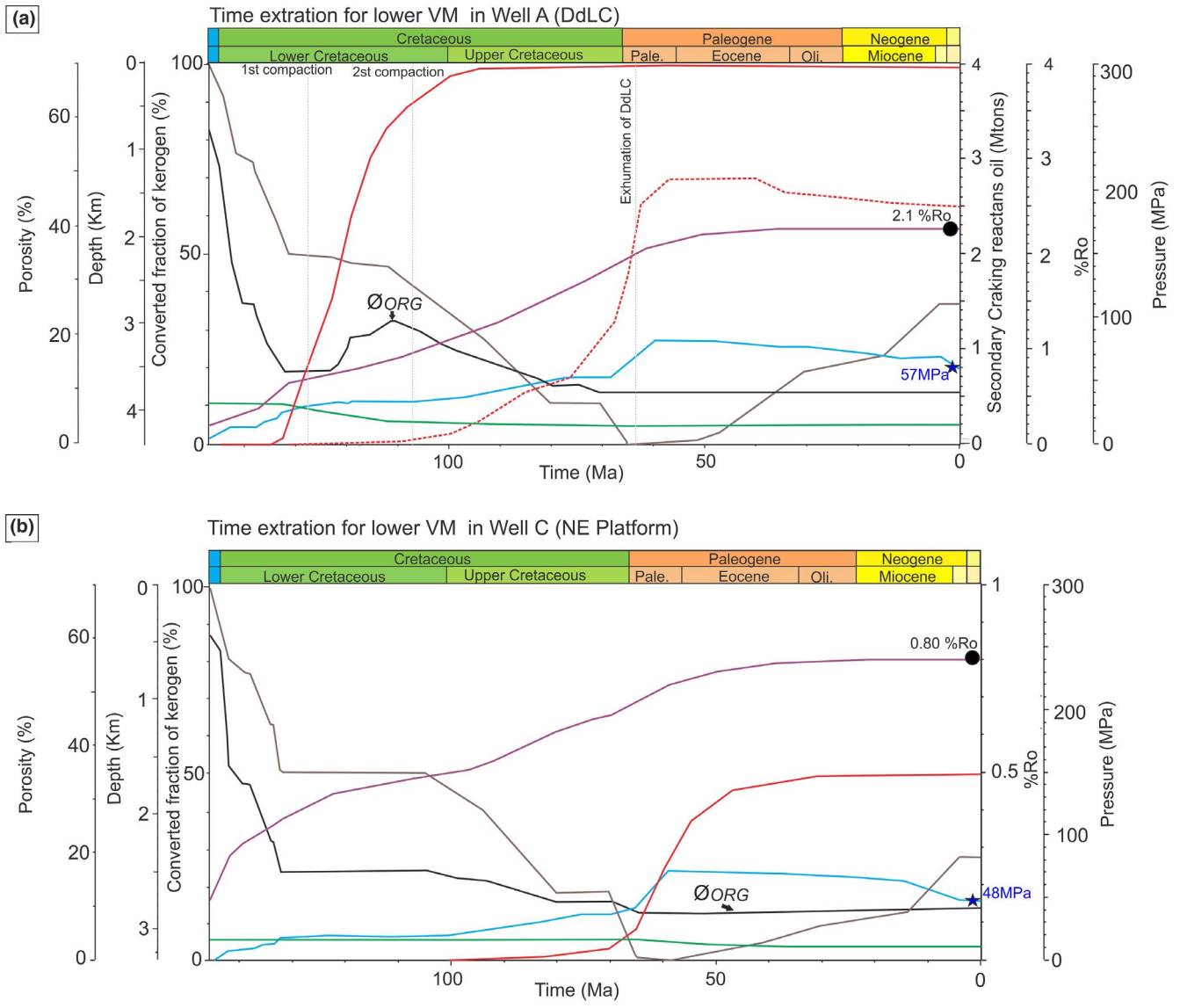

FIGURE 11 Time extractions for the lower VM in the Agrio model. (a) DdLC and (b) NE Platform areas. Curve references: Transformation ratio (red), burial depth (brown), vitrinite reflectance (violet), total porosity (black), TOC (green), pore pressure (light blue) and secondary cracking mass (dashed red). Present-day vitrinite reflectance values (black circles), pressure data derived from DFIT tests (blue stars) and the onset of organic porosity (Øorg) development are included in both extractions

decreasing temperature and pressure. This process likely promoted a reduction in pore pressure associated with the expulsion of large amounts of gas from the Jurassic and Lower Cretaceous source rocks. The structural duplication in the outer sector resulted in a component of structural thickening, which promoted thermal reactivation and, consequently, increase in secondary cracking reactions and pore pressure. Towards the structural heights of DdLC, the Los Molles source rock was also overmature (>4 %Ro), and the lower VM reached the gas window (2 %Ro).

Present-day maturity shows that the Los Molles and VMFms are completely exhausted from the inner sector to the eastern flank of the DdLC (Figure 10d). Towards the DdLC area, the calculated maturity trend for Well A shows that the lower VM reached the dry gas window (Figures 9b and 10d). Furthermore, the model predicts that in the NE platform area, the lower VM is in the early-to-peak oil window and reaches a transformation ratio of 50% (Figure 10d). Simulated and calculated vitrinite reflectance values show a clear decrease from the Agrio FTB to the foreland (east) region of the basin.

6.3 | Time extractions for the lower Vaca Muerta in the DdLC and NE Platform areas

The interplay of key processes related to regional tectonic events and hydrocarbon generation, thermal stress, pore pressure and porosity development was analysed in time

extractions for the lower VM in the DdLC and NE Platform areas of the Agrio section (Figure 11).

The DdLC area shows that during the Early Cretaceous the lower VM underwent a first phase of burial compaction (brown curve in Figure 11a), which reduced the effective porosity from 60% to 13% (black curve in Figure 11a). Pore pressure increased up to 28 MPa (blue curve in Figure 11a) interpreted to result from incomplete drainage of generated fluids. From ca. 120 Ma, the unit reached a TR of 88% (red curve in Figure 11a), which induced an abrupt increase in the porosity (black curve in Figure 11a) related to the growth of Øorg. The model also shows that the development of Øorg added ca. 11% to the porosity and reduced the TOC content to ca. 5% (green curve in Figure 11a). Furthermore, continuous thermal cracking increased pore pressure, which induced a first pulse of petroleum expulsion at thermal maturity of 0.82 %Ro (violet curve in Figure 11a). A second phase of mechanical compaction started at ca. 100 Ma and caused a reduction in porosity, likely including both matrix and organic porosity (black curve in Figure 11a). At ca. 65 Ma, the unit reached maximum burial (brown curve in Figure 11a) and the effective porosity was reduced to 10%. Secondary cracking reactions, accompanied by gas generation (dashed red curve in Figure 11a), caused an increase in pore pressure of ca. 87 MPa. From ca. 50 Ma, progressive uplift of the DdLC anticline started and continued during Palaeocene, Eocene and Miocene times. Uplift and consequent erosion reduced vertical stress, thereby reducing the required pore pressure to maintain equilibrium with the overlying column. This is demonstrated in the model between 50 Ma and present-day when about 500 m of section was eroded, which led to a decline in pore pressure (blue curve in Figure 11a). By present-day the pore pressure dropped to 57 MPa, which is consistent with DFIT values obtained in Well A (violet star in Figure 11a).

In the NE Platform, the lower VM underwent a continuous decrease in effective porosity from 58% to 7% (black curve in Figure 11b) due to mechanical compaction that took place between 150 and 60 Ma. At 60 Ma, TR of 45% (red curve in Figure 11b) shows that most of the unit was in the main oil window during the maximum burial (brown curve in Figure 11b). The model shows that increased burial depth and hydrocarbon generation increased the pore pressure (blue curve in Figure 11b) to ca. 62 MPa. From ca. 22 Ma to present day, progressive uplift and erosion reduced the pore pressure from 60 to 48 MPa, which is comparable with DFIT measures for Well C (violet star in Figure 11b). Progressive transformation of OM occurred in parallel with the reduction in TOC contents (green curve in Figure 11b) and increased porosity (black curve in Figure 11b), which is interpreted as a product of Øorg development. The Øorg added 2.2% to the effective porosity in the lower VM. The simulations allow us to recognize significant differences in Øorg development between the DdLC (11%) and NE Platform (2.2%), which correlate with TOC_0 variations and transformation gradient. In the DdLC area, the high TOC_0 concentration associated with a high transformation ratio promoted an increase in Øorg development compared with the NE Platform.

7 | DISCUSSION

7.1 | Organic geochemical pattern in the VMFm

Regional studies of the VMFm have examined the OM distribution, including richness (quantity), free hydrocarbons

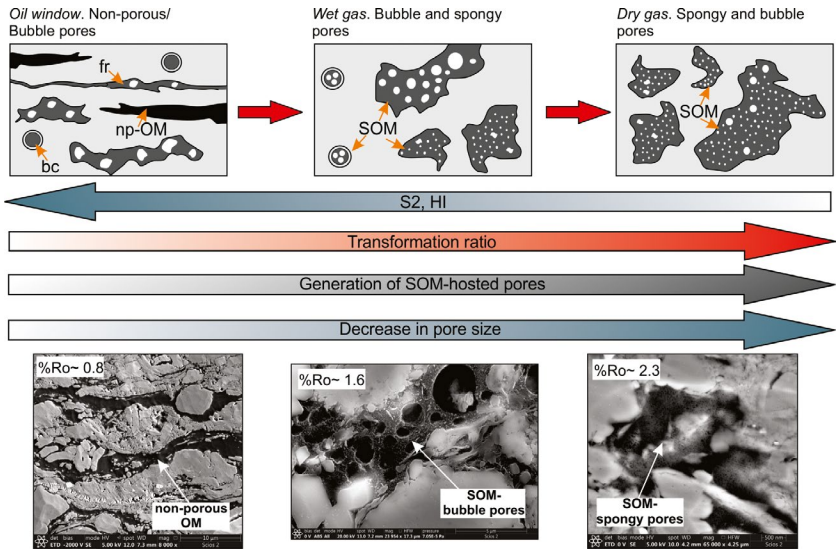

FIGURE 12 Schematic evolution of organic matter pore types with increased thermal maturity based on SEM and pyrolysis data for the VMFm. References: np-OM (nonporous organic matter), bc (bioclasts), fr (fracture) and SOM (secondary organic matter)

and thermal maturity (e.g. TR, %Ro) of the unit (e.g. Brisson et al., 2020; Cruz et al., 1996, 2002; Legarreta & Villar, 2011, 2015; Urien & Zambrano, 1994; Veiga et al., 2020). In addition, there are many local contributions from outcrop sections and the subsurface that include TOC and Rock-Eval® pyrolysis analyses (e.g. Askenazi et al., 2013; Boll et al., 2014; Capelli et al., 2021; Cavelan et al., 2019; Karg & Littke, 2020; Krim et al., 2019; Małachowska et al., 2019; Milliken et al., 2019; Petersen et al., 2020; Romero-Sarmiento et al., 2017; Scasso et al., 2005; Sylwan, 2014). All those studies and the present work indicate high present-day TOC values ranging from 1% to 12% with maximum values towards the base of the unit in the lower VM (Figure 4). However, present-day TOC content may not reflect the loss of organic carbon during thermal maturation. Thus, the original TOC_0 based on the reconstruction of Brisson et al. (2020) is a suitable parameter to examine vertical and lateral richness distribution (Figure 4), and it is applicable for the VMFm. In the Agrio section, the lower VM shows an increase in TOC_0 values from 6% (east) to 8% (west). This observation is consistent with the westward facies deepening of classic palaeogeographic maps accompanied by restricted settings under low-oxygen water conditions that favour preservation of OM (Legarreta & Uliana, 1991). The increase in TOC values from east to west is associated with thickening of the VMFm between ca. 400 and 800 m in the same trend (Dominguez et al., 2016), which means a higher volume of generated hydrocarbons for the same gradient of TR. Notably, Well B shows the highest present-day (mean 8%) and original TOC (mean 18% for the lower VM) contents, which suggests that local effects could have influenced these positive anomalies. As analysed by Dominguez et al. (2016), organic-rich intervals in the VMFm correspond to bottomset–distal foreset segments of prograding clinoforms, conditioned by stratigraphic and in some cases tectonic (differential subsidence and palaeo-arch uplift) controls. The lower VM exhibits mostly stratigraphic controls (Dominguez et al., 2016), and therefore, a position close to the distal foreset is envisaged where optimal conditions for the production and preservation of OM occurred (Passey et al., 2010).

OM in the unit shows negligible compositional differences, both geographically and stratigraphically, and is typically described as unstructured algal material (type II kerogen) with very scarce land-derived (e.g. vitrinite) particles that yielded an estimated HI_0 of 680 mg_{HC}/g_{TOC} (Brisson et al., 2020; Petersen et al., 2020; Veiga et al., 2020). As recorded in the Agrio section, the basin shows an E–W thermal gradient, which is consistent with the decrease in HI (Figure 5) and increase in TR values to the west. The sample set exhibits a gradual decrease in HI with increasing maturity gradient from 470 mg_{HC}/g_{TOC} (general average for the early oil window, Well C) to 41 mg_{HC}/g_{TOC} (general average for the early oil window, Well A). This denotes the transformation of type II kerogen into hydrocarbons and the concomitant reduction in HI (Hazra et al., 2019; Peters & Cassa, 1994).

Some samples from the upper VM show an increase in OI, which could suggest some terrigenous OM input; however, it may be better to interpret it as the result of OM oxidation during transport and deposition (Peters, 1986). In the case of the upper VM, that increase is accompanied by a decline in TOC content related to the shallowing upward tendency of this interval. As the upper VM shows an increase in the carbonate content (Capelli et al., 2021; Legarreta & Villar, 2015), impure calcite could also generate some CO_2 upon pyrolysis and, as a consequence, an increase in the S3 peak and OI parameter (Peters, 1986).

7.2 | Evolution of OM across the maturation gradient

The importance of shale reservoirs as sources of oil and gas has motivated numerous studies that focus on parameters that control the development and preservation of pores (Katz & Arango, 2018; Ko et al., 2017; Liu et al., 2017; Löhr et al., 2015; Milliken et al., 2013; Reed & Loucks, 2015). The regional analysis of the VMFm presented in this work demonstrates that maturity is an important factor that impacts the development of Øorg. The early and rapid changes in TR that characterize type II kerogen from the VMFm (Brisson et al., 2020) suggest that OM-hosted pores are associated with partially and exhausted OM generated during primary and secondary cracking reactions. As also documented by Tomassini et al. (2019), the general high TOC content of the unit indicates that OM-hosted pores are the main storage of potential fluids.

In the oil window and based on TR and SEM data, the OM that hosts pores is partially transformed and occupies spaces between detrital grains, the internal structure of bioclasts and fractures (Figure 12). Interestingly, some samples from the early oil window (Well C) lack OM-hosted pores and have the lowest values of TR (mean 30%, Table 1). Filament-like organic particles resemble those liptinite macerals identified under optical petrography in immature to low mature samples (Brisson et al., 2020; Małachowska et al., 2019; Petersen et al., 2020). The type II sapropelic kerogen that prevailed during sedimentation of the VMFm (Brisson et al., 2020; Legarreta & Villar, 2015) is prone to ductile compaction (Figure 6a–c) and loss of primary porosity (Löhr et al., 2015; Milliken et al., 2014). In analogous shale units at low thermal maturity, type II kerogen is nonporous and highly affected by mechanical compaction (Comerio et al., 2020; Schieber, 2013). This observation indicates that the potential infill of pores in this early-generation stage with heavy, bitumen-like petroleum (Petersen et al., 2020) could explain why liptinite macerals do not show evidence of pores at SEM resolution (Löhr et al., 2015). However, at some rock

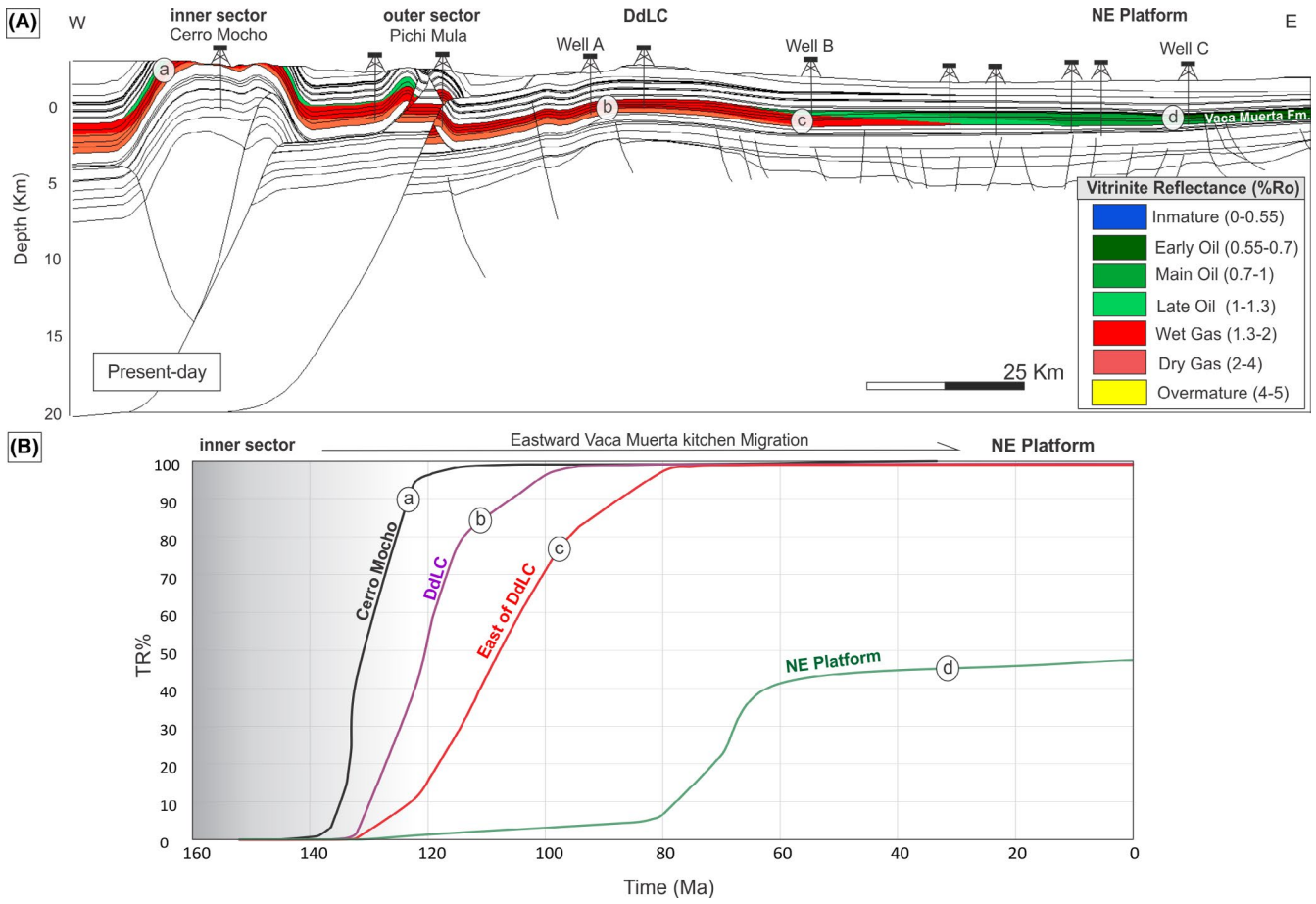

FIGURE 13 (A) Present-day maturity (%Ro) of the VMFm along the Agrio section. (B) Thermal maturity based on transformation ratio (TR%) for the lower VM is presented in four areas: (a) Cerro Mocho, (b) DdLC, (c) East of DdLC and (d) NE Platform

intervals in the early oil window, isolated bubble pores occur in secondary OM products (e.g. solid bitumen), suggesting that other processes were involved in the development of Øorg. As was pointed out by Brisson et al. (2020), variations in depositional conditions could have influenced the final composition of oil-prone organofacies (e.g. sulphur-rich vs. sulphur-depleted). These diagenetic differences could affect the onset of primary cracking reactions and the generation of liquid hydrocarbons and bitumen (Hackley & Cardott, 2016). Thus, decomposition of kinetically distinct kerogens at different rates might explain why that some strata at the same thermal maturity preserve nonporous liptinite macerals, whereas in others Øorg is associated with secondary OM products such as the solid bitumen.

OM-hosted pores in the gas window are interpreted to develop in secondary, highly transformed (TR > 90%) OM and show both the bubble and spongy morphologies (Ko et al., 2017; Milliken et al., 2013). The wet gas window (Well B) exhibits the largest bubble pores (2–4 μm) associated with development of highly concentrated spongy pores that are absent in the early oil window but become more abundant in the dry gas window (Figure 12). Large bubble pores occur in 'shelter' pores (Figure 7a–c), such as in the interior of bioclasts and around diagenetic products (calcite cement) indicating that some lithologies (Milliken et al., 2019) favoured their preservation. They likely formed in the oil window as was interpreted for the Eagle Ford Fm (Cenomanian–Turonian, Maverick Basin of south Texas), where bubble pores include hydrocarbon liquids that were left behind or migrated following petroleum generation (Schieber et al., 2016). Consequently, we interpret that spongy pores started to grow during secondary cracking due to decomposition of partially transformed OM by thermal maturity. Some bubble pores appear to form due to coalescence of spongy pores (Figure 8c,d) and were, therefore, also generated during the dry gas window (Cavelan et al., 2019). The bubble geometry is mainly represented by macropores (pore sizes >50 nm) and well documented with SEM resolution. On the contrary, spongy pores include a part of mesopores (2–50 nm) and presumably micropores (<2 nm), the latter measured through nitrogen adsorption analysis by Cavelan et al. (2019) for the VMFm. For terrigenous OM, SEM does

not show pores at any maturity, the same observations apply for the New Albany Shale (Devonian–Mississippian, Illinois Basin at USA), where vitrinite and inertinite macerals may not contribute to additional Øorg (Liu et al., 2017).

SEM images do not show clear evidence of deformed organic pores; except for some examples in Well B where OM-hosted pores within a clay-rich matrix exhibit elongated (flattened) forms interpreted as the product of mechanical compaction (Figure 7e). Previous studies documented that organic pores can survive mechanical compaction but preserve features of OM deformation (Wang, 2020). As documented for the VMFm, most organic pores are preserved showing circular forms, which implies that rigid components such as microfossils and diagenetic products (microcrystalline quartz and calcite cement) inhibit the effects of compaction. In addition, the analysed samples are far from intensively deformed areas (e.g. outcrops in the internal belts) where OM-hosted pores could be deformed. The OM-hosted pores are interpreted to result from kerogen and bitumen cracking to oil and gas, presumably in equilibrium between lithostatic pressure and pore pressure within the unit (Ko et al., 2017). Accordingly, overpressure-related processes could represent important mechanisms that inhibit the effects of compaction and contributed to preservation of Øorg (see Section 7.3.3).

7.3 | BPSM in the Agrio cross section

The 2D modelled section presented in this work reproduces the decrease in maturity and OM transformation from west (fold and thrust belt) to east (basin margin) for the main source rocks in the Neuquén Basin (see Section 6). For the VMFm, the models predict temporal and spatial variations in the timing of hydrocarbon generation–expulsion controlled by tectonic events, burial depth and differences in thickness of the Mesozoic sedimentary overburden. Model results show that OM transformation impacted on the magnitude of (a) the effective porosity associated with Øorg development, and (b) the distribution of pore pressure within the unit.

7.3.1 | Timing of hydrocarbon generation

Based on present-day %Ro values, maturity windows of the VMFm along the Agrio section are presented in Figure 13. Temporal and spatial variations in the timing of kerogen transformation are documented between the inner sector and the NE Platform. From the fold belt (Cerro Mocho–Pichi Mula) to the DdLC structure, the lower VM reached the dry gas window, and according to the modelling, the maximum transformation occurred at ca. 120 Ma in the inner sector (A-curve in Figure 13b) before the Late Cretaceous Andean deformation phase that affected the western part of the belt (Cobbold & Rossello, 2003; Rojas Vera et al., 2015; Sánchez et al., 2018; Zamora Valcarce et al., 2011; Zapata & Folguera, 2005). Modelling results indicate that hydrocarbon generation and expulsion preceded the growth of main structures in the inner and outer sectors of the Agrio FTB and would have been favoured by the increase in the Mesozoic sedimentary cover towards the inner and outer sectors (ca. 4–5 km burial depth). Nevertheless, tectonic uplift and cooling of both sectors correlate with the Miocene contractional pulse. As a consequence, thermal stress and secondary cracking stopped, and pore pressure decreased, since remnant fluids (mainly gas) were expelled from the unit. Such interpretations were previously inferred by Gómez Omil et al. (2014), indicating that intensely deformed areas in the Neuquén Basin are at present day inactive and incapable of generating hydrocarbons.

For the DdLC structure, TR of 99% shows that the lower VM was already in the dry gas window at ca. 98 Ma (B-curve in Figure 13b), whereas in the external flank of this structure full transformation conditions were reached at ca. 80 Ma (C-curve in Figure 13b). Compressive deformation and uplift/regional erosion promoted the exhumation of the unit associated with expulsion of fluids as well as hydrocarbon migration and trapping in previously generated structures (Rocha et al., 2018). This observation is consistent with our modelling because the dissipation of pore pressure (blue curve in Figure 11a) and fluid expulsion are linked to exhumation events that occurred mainly between Palaeocene and Miocene time. The NE Platform shows that the unit reached the early-to-peak oil window with a TR of 40%–50%, indicating that hydrocarbons generation started from ca. 60 Ma (D-curve in Figure 13b).

The model indicates that hydrocarbon generation and expulsion started in the western VMFm before the Late Cretaceous Andean deformation, which controlled the uplift of inner sectors within the Agrio FTB. In the undeformed scenario (Figure 10a), hydrocarbons were able to migrate up to 70 km through the main carrier beds in the basin (Cruz et al., 2002; Rocha et al., 2018). At present day, the VMFm is totally exhausted in the intensely deformed regions of the belt, with full kerogen transformation into hydrocarbons at ca. 120 Ma. At the basin scale, the Agrio model shows a clear eastward decrease in maturity and transformation gradient associated with changes in the sedimentary column thickness that led to differential maximum burial before the Miocene deformation pulse. Similar interpretations were documented along the Chos Malal FTB, where thermal maturity and transformation also decrease eastward linked to differences in thickness of the sedimentary overburden (Cruz et al., 1996; Karg & Littke, 2020). In the inner sector of the Agrio FTB, the Miocene uplift caused present-day source rocks to show relict maturity reached at deeper burial depths in the past. In addition, there is an increase in the thermal stress and transformation of the OM from north to south, mainly controlled

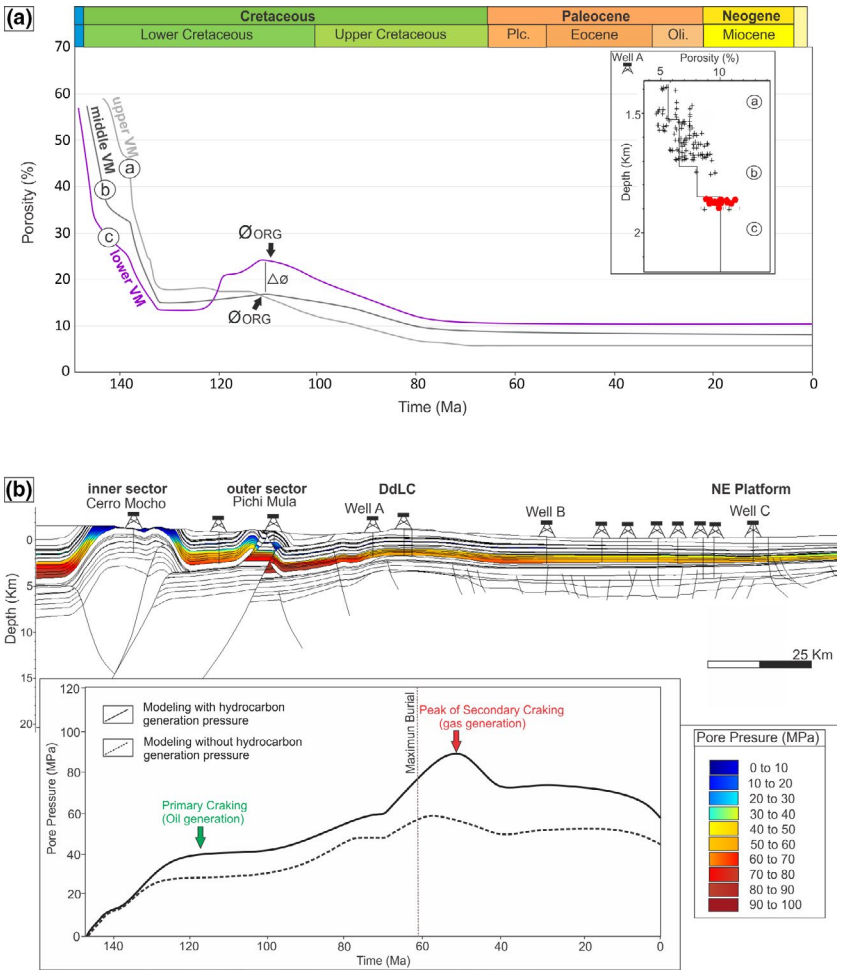

FIGURE 14 (a) Effective porosity curves through geologic time for the lower, middle and upper VM in DdLC (Well A). Simulated porosity increases as a response to organic porosity (Øorg) development and the porosity difference between upper and lower VM is expressed as ΔØ. Modelling indicates a progressive increase in porosity from the top to the base of the unit related to TOC_0 and thermal maturity increase and, therefore, with increase in Øorg in the same trend. The insert shows the calculated porosity (black curve) and data obtained from well logging (black cross) and gas-filled porosity (red circles) from core samples. (b) Distribution of present-day pore pressure in the VMFm. Pore pressure modelling for the lower VM in Well A with (black curve) and without hydrocarbon generation (dashed black curve)

increased sedimentary thickness in the same trend (Gómez Omil et al., 2014; Legarreta et al., 2008). These observations indicate that the effects of thermal maturity follow a N–S trend controlled by a general thickness increase in the source rocks of the Mendoza Group towards the area of the Agrio FTB, to the north of the Huincul Arch (see location in Figure 1).

7.3.2 | Organic porosity estimation

The integrated modelling results and SEM images indicate that the development of Øorg is a typical feature of the VMFm. Petromod® software calculates Øorg as the result of OM transformation from solid immature kerogen to less dense fluid hydrocarbons during thermal maturation (Hantschel & Kauerauf, 2009). Time extractions show an increase in effective porosity, interpreted as the result of Øorg linked to the transformation of OM into hydrocarbons (Figure 14a). The simulations are comparable with those of Modica and Lapierre (2012): Øorg tends to increase with burial depth and thermal transformation. Accordingly, Øorg differences for the lower VM between the DdLC (11%) and NE Platform (2.2%) correspond to an increase in TR values to the west in the basin. Such observations are consistent with basin-scale modelling of Øorg in the Mississippian Barnett Shale that allowed Romero-Sarmiento et al. (2013) to estimate from 0% (immature zones) to 4% Øorg (mature zones) of rock volume. However, as for the Upper Devonian Duvernay Formation in the Western Canada Basin (Chen & Jiang, 2016), the development of Øorg is also a function of TOC_0 and kerogen type, since type I kerogen generates more Øorg than type III kerogen (Chen et al., 2015).

Time extractions show variations in the effective porosity through time for the lower, middle and upper VM in Well A (Figure 14a). From 120 Ma, the lower VM (TOC_0 11% average) increased its porosity by ca. 11%, which is interpreted as a response to Øorg development. The curve obtained by Mei et al. (2021) for the VMFm also shows a considerable increase in porosity due to Øorg development associated with the onset of hydrocarbon generation. To the contrary, the upper VM (TOC_0 2% average) would have developed only 1.95% of Øorg at full transformation, a value that does not considerably affect the evolution of the porosity curve (Figure 14a). Time extractions indicate progressive increase in porosity from the top to the base of the unit related to TOC_0 and thermal maturity and, therefore, with the

increased in Øorg in the same trend. This observation agrees with SEM analysis, which found that OM-hosted pores are dominant in organic-rich intervals of the unit (Tomassini et al., 2019). Although it is beyond the scope of this study to quantify the porosity, our results suggest that organic-rich intervals of the VMFm and associated OM pores control the hydrocarbon storage capacity. Similar results have been documented in other worldwide class unconventional resources, as in the Barnett (Texas) and Haynesville (Texas, Arkansas, Louisiana) Fms, where much of the petroleum is trapped in organic pores (Passey et al., 2010; Peters et al., 2017; Romero-Sarmiento et al., 2013).

It is important to highlight that the constructed model incorporates bulk kinetics specific for the VMFm (Brisson et al., 2020), which provided accurate information on thermal evolution of the OM, Øorg and timing of hydrocarbon generation. Future investigations should incorporate detailed compositional kinetic schemes to optimize the evolution of TOC, Øorg and hydrocarbon retention and expulsion in the VMFm (see Mei et al., 2021).

7.3.3 | Pore pressure related to hydrocarbon generation

2D basin modelling suggests that hydrocarbon generation represents an important mechanism that controls the magnitude and distribution of pore pressure in the VMFm. Simulations and DFIT data indicate that the unit is an overpressured system at different basin positions. Previous studies proposed that the transformation of kerogen into oil and gas represents the main mechanism for overpressure generation in the VMFm (Badessich et al., 2016; Cobbold et al., 2013; Rocha et al., 2018; Rodrigues et al., 2009; Veiga et al., 2020; Zanella et al., 2015). The volume expansion associated with hydrocarbon generation has been implicated as a cause of overpressure in different sedimentary basins (Osborne & Swarbrick, 1997; Swarbrick et al., 2002). Hydrocarbon generation can be a cause for overpressure if the rate of volume increase due to kerogen transformation exceeds the rate of volume loss by fluid expulsion and migration (Berg & Gangi, 1999). Bredehoeft et al. (1994) proposed that if the liquid generated during thermal cracking is less dense than the solid kerogen, then there will be more liquid than created pores and, thus, the pore pressure will increase. This overpressure mechanism depends upon kerogen type, abundance of OM, thermal history and rock permeability (Osborne & Swarbrick, 1997). For the VMFm, modelling results show that pore pressure magnitude was influenced by abundance of OM and generated fluids, both parameters controlled by the position in the basin and thermal history. The highest pore pressures coincide with the western part of the basin, where the VMFm shows highest TOC_0 contents and where the unit reached the gas window. Osborne and Swarbrick (1997) suggested that changes in overpressure gradients related to volume expansion after hydrocarbon generation are controlled by two main reactions: (1) low-temperature reaction rate for primary cracking of kerogen into oil and gas, and (2) high-temperature reaction rate for secondary cracking of oil and bitumen into gas. In particular, secondary cracking reactions induce a significant overpressure within low permeability source rocks (Osborne & Swarbrick, 1997). High pressures are more readily developed by gas generation than by oil generation because of the much lower density of gas (Barker, 1990). Different case studies documented that the generation of gas resulted in conditions of overpressure within source rocks (Carcione & Gangi, 2000; Gao et al., 2019; Hao et al., 1996; Hunt, 1990; McPeek, 1981; Nunn, 2012; Ramdhan & Goulty, 2010; Swarbrick et al., 2002; Tingay et al., 2009). Cracking of 1 vol% of oil would generate overpressures close to the magnitude of the lithostatic gradient in confined rocks (Barker, 1990). The relationship between pore pressure and maturity windows for the VMFm along the Agrio FTB is shown in Figure 14b. Well A (DdLC) in the gas window at present day reaches 57 MPa, whereas towards the oil window (Well C), the pore pressure reaches 48 MPa. The volume expansion related to primary and secondary cracking would have controlled such differences in pore pressure of the VMFm between different maturity stages. These results indicate that secondary cracking of retained hydrocarbons in VMFm produced a significant increase in pore pressure in western areas of the Neuquén Basin.

The Petromod® software calculates the pore pressure caused by primary and secondary cracking reactions considering different parameters such as kerogen reduction, porosity, density of hydrocarbons and compressibility (Hantschel & Kauerauf, 2009). The magnitude of fluid expansion on pore pressure was also evaluated in a model excluding hydrocarbon generation in pore pressure calculations for the VMFm in the DdLC area (Figure 14b). Interestingly, the two models show discrepancies in the magnitude of pore pressure, confirming that hydrocarbon generation, especially gas, plays a significant role in pressure generation. In the second model, pore pressure generation was related to disequilibrium compaction and pore pressure magnitude is lower than the model with hydrocarbon generation. In particular, during the peak of gas generation (ca. 50 Ma), the pore pressure difference is ca. 30% on average between both models (Figure 14b). Our results suggest that both disequilibrium compaction and hydrocarbon generation could act as coupled processes contributing to pore pressure generation within the VMFm.

On the other hand, the present-day distribution of pore pressure (Figure 14b) depends on the magnitude of different processes that reduce pore pressure such as fracturing, uplift and erosion (Doré & Jensen, 1996; Law & Dickinson, 1985; Law & Spencer, 1998; Neuzil & Pollock, 1983). Such

processes reduce vertical stress, thereby reducing the required pore pressure to maintain equilibrium with the overlying column (Burgreen-Chan et al., 2015). Pore pressure reduction is recorded in the time extraction for DdLC when ca. 1,000 m of sedimentary rocks were eroded from 65 Ma to present day. The pore pressure in the unit decreases from 87 MPa (50 Ma) to 57 MPa (present day), demonstrating the capacity of fracturing, uplift and erosion to reduce pressure and promote late expulsion and migration of hydrocarbons into potential traps. The amount of pore pressure reduction appears to be a consequence of the permeability increase triggered by fracturing, uplift and erosion associated with a decrease in lithostatic load. In the same way, the Miocene tectonic uplift stopped the thermal stress and secondary cracking, thus promoting a substantial pore pressure reduction in the Agrio Fold belt. The reduction in pore pressure in the VMFm associated with those processes is in agreement with observations and modelling from other studies in the unit (Mei et al., 2021). We consider that tectonic uplift could be an important process for redistribution of hydrocarbons within the basin and individual traps because of changes in structural configuration (e.g. Shanley & Cluff, 2015). In the model, the faults were assumed to be closed (i.e. impermeable) for the simulated steps. Compartmentalization due to faults is a common feature in petroleum systems and, in many cases, is identified by laterally different pressure regimens (Borge, 2002; Borge & Sylta, 1998; Gibson & Bentham, 2003; Williams & Madatov, 2005). This is documented in the Pichi Mula triangular zone, where closed faults inhibited the drainage of fluids and resulted in high present-day pressure (Figure 14b).

Finally, 2D basin modelling by Berthelon et al. (2021) suggested that horizontal (tectonic) compression related to Andean deformation could increase overpressure in the VMFm. However, the authors mentioned that their proposed model does not integrate horizontal stress with hydrocarbon generation in the calculation of the overpressure. The modelling in our study shows that generation of hydrocarbons and compaction disequilibrium represents the main mechanisms controlling overpressure in the VMFm. However, we do not rule out the possibility that compressional stress related to Andean deformation may have also influenced the distribution and magnitude of pore pressure. This proposal should be modelled in detail considering the magnitudes and temporal relationships among maximum burial, hydrocarbon generation and horizontal stress.

8 | CONCLUSIONS

This study analyses the unconventional petroleum potential of the VMFm source rock at different thermal maturities based on organic geochemistry, electron microscopy and a regional BPSM from the Agrio FTB to the basin border. A robust data set was incorporated into the model with the purpose of integrating regional tectonic events and processes that controlled the generation and expulsion of hydrocarbons, organic porosity development and pore pressure mechanisms through geologic time.

In the Agrio FTB, the lower Vaca Muerta shows an increase in TOC_0 towards the west from 4% to 8% mean values. The increase in TOC_0 from east to west is associated with thickening of the unit, which suggests the potential larger volumes of generated hydrocarbons for the same thermal gradient. Thermal maturity based on the transformation ratio (TR) controlled the development of organic pores. TR increases westward, indicating that in conjunction with increased TOC_0, organic pores represent the main control on total porosity in organic-rich intervals of the unit. Along the Agrio FTB, ca. 11% of organic porosity was reached in the DdLC (gas window), whereas only ca. 2% was reached in the NE Platform (early oil) for the lower Vaca Muerta. Organic geochemistry and electron microscopy demonstrate that OM-hosted pores are related to thermal degradation of oil-prone type II kerogen into partially (TR ca. 3%–60%) nearly completely (TR ca. 80%–99%) transformed OM. Based on SEM images, isolated bubble pores are typical of the oil window, whereas bubble and densely distributed spongy pores occur in the gas window.

BPSM shows that temporal and spatial variations in the timing of hydrocarbon generation are linked to tectonic events, burial depth and differences in thickness of the Mesozoic sedimentary overburden. The model shows a clear decrease in maturity and OM transformation to the east (basin margin) for the main source rocks in the Neuquén Basin. 2D modelling predicts that large volumes of hydrocarbons were generated and expelled from VMFm during the Early and Late Cretaceous in western sectors of the basin.

The VMFm is an overpressure cell at different basin positions. BPSM indicates that hydrocarbon generation and compaction disequilibrium were main mechanisms that controlled magnitude and distribution of pore pressure. The volume expansion associated with hydrocarbon generation reached maximum values from secondary cracking (transformation of oil and bitumen into gas) during the Late Cretaceous–Palaeocene.

The distribution of OM and mechanisms that control pressure and porosity along the maturity gradient represent key parameters to evaluate unconventional plays in the context of basin evolution. In the Vaca Muerta Formation, overpressure intervals with high organic carbon contents are the most prone to develop organic pores, which represent favourable sites for the storage of hydrocarbons.

ACKNOWLEDGEMENTS

This study is published with the permission of YPF and YTEC. We are especially grateful to L. Monti, G. Sagasti and R. Manoni (YPF), C. Smal and J. P. Alvarez (Y-TEC) for allowing us to publish the present data. To M. Fasola, for his review and constructive comments. Special thanks to A. Floridia, N. Jausoro and F. Medina (Laboratorio de Microscopía in Y-TEC) for SEM analysis. H. Villar (GeoLab Sur) is thanked for pyrolysis analysis and vitrinite determinations. Special thanks to M. F. Romero-Sarmiento and B. Katz who provided thoughtful comments and further improved this article. We also express our gratitude to K. Peters for his useful edits, suggestions and ideas. We acknowledge C. Jhonson (Asociate Editor of BR) for constructive comments on the original version of the manuscript.

PEER REVIEW

The peer review history for this article is available at https://publons.com/publon/10.1111/bre.12599.

DATA AVAILABILITY STATEMENT

The data that support the findings of this study are available from the corresponding author upon reasonable request.

REFERENCES

Aguirre-Urreta, B., Tunik, M., Naipauer, M., Pazos, P., Ottone, E., Fanning, M., & Ramos, V. A. (2011). Malargüe Group (Maastrichtian–Danian) deposits in the Neuquén Andes, Argentina: Implications for the onset of the first Atlantic transgression related to Western Gondwana break-up. *Gondwana Research*, *19*, 482–494. https://doi.org/10.1016/j.gr.2010.06.008

Aguirre-Urreta, M. B., Mourgues, F. A., Rawson, P. F., Bulot, L. G., & Jaillard, E. (2007). The Lower Cretaceous Chañarcillo and Neuquén Andean basins: Ammonoid biostratigraphy and correlations. *Geological Journal*, *42*, 143–173. https://doi.org/10.1002/gj.1068

Al-Hajeri, M. M., Saeed, M. A., Derks, J., Fuchs, T., Hantschel, T., Kauerauf, A., Neumaier, M., Schenk, O., Swientek, O., Tessen, N., Welte, D., Wygrala, B., Kornpihl, D., & Peters, K. (2009). Basin and petroleum system modeling. *Oilfield Review*, *21*, 14–29.

Askenazi, A., Biscayart, P., Cáneva, M., Montenegro, S., & Moreno, M. (2013). *Analogía entre la Formación Vaca Muerta y shale gas/oil plays de EEUU*. Society of Petroleum Engeneers (SPE).

Athy, L. F. (1930). Density, porosity, and compaction of sedimentary rocks. *AAPG Bulletin*, *14*, 1–24.

Badessich, M. F., Hryb, D. E., Suarez, M., Mosse, L., Palermo, N., Pichon, S., & Reynolds, L. (2016). Vaca Muerta shale—Taming a giant. *Oilfield Review*, *28*, 26–39.

Bakar, R. (2018). *Modeling and analysis of diagnostic fracture injection tests (DFITs)* (M.Sc. Thesis). Department of Petroleum Engineering, Colorado School of Mines.

Barker, C. (1990). Calculated volume and pressure changes during the thermal cracking of oil to gas in reservoirs. *AAPG Bulletin*, *74*, 1254–1261.

Berg, R. R., & Gangi, A. F. (1999). Primary migration by oil-generation microfracturing in low-permeability source rocks: Application to the Austin Chalk, Texas. *AAPG Bulletin*, *83*, 727–756.

Berthelon, J., Brüch, A., Colombo, D., Frey, J., Traby, R., Bouziat, A., Cacas-Stentz, M. C., & Cornu, T. (2021). Impact of tectonic shortening on fluid overpressure in petroleum system modelling: Insights from the Neuquén basin, Argentina. *Marine and Petroleum Geology*, *127*, 104933.

Boll, A., Alonso, A., Fuentes, F., Vergara, M., Laffitte, G., & Villar, H. J. (2014). Proceedings of IX Congreso de Exploración y Desarrollo de Hidrocarburos, Mendoza, Argentina, Actas (pp. 3–44).

Borge, H. (2002). Modelling generation and dissipation of overpressure in sedimentary basins: An example from the Halten Terrace, offshore Norway. *Marine and Petroleum Geology*, *19*, 377–388. https://doi.org/10.1016/S0264-8172(02)00023-5

Borge, H., & Sylta, Ø. (1998). 3D modelling of fault bounded pressure compartments in the North Viking Graben. *Energy Exploration and Exploitation*, *16*(4), 301–323.

Bredehoeft, J. D., Wesley, J. B., & Fouch, T. D. (1994). Simulations of the origin of fluid pressure, fracture generation, and the movement of fluids in the Uinta Basin, Utah. *AAPG Bulletin*, *78*(11), 1729–1747.

Brisson, I. E., Fasola, M. E., & Villar, H. J. (2020). Organic geochemical patterns of the Vaca Muerta Shale. In D. Minisini, M. Fantin, I. Lanusse, & H. Leanza (Eds.), *Integrated geology of unconventionals: The case of the Vaca Muerta play, Argentina*. AAPG Memoir 120, Chapter 11.

Burgreen-Chan, B., Meisling, K. E., & Graham, S. (2015). Basin and petroleum system modelling of the East Coast Basin, New Zealand: A test of overpressure scenarios in a convergent margin. *Basin Research*, *28*, 536–567. https://doi.org/10.1111/bre.12121

Capelli, I. A., Scasso, R. A., Spangenberg, J. E., Kietzmann, D. A., Cravero, F., Duperron, M., & Adatte, T. (2021). Mineralogy and geochemistry of deeply-buried marine sediments of the Vaca Muerta-Quintuco system in the Neuquén Basin (Chacay Melehue section), Argentina: Paleoclimatic and paleoenvironmental implications for the global Tithonian-Valanginian reconstructions. *Journal of South American Earth Sciences*, *107*, 103103.

Carcione, J. M., & Gangi, A. F. (2000). Gas generation and overpressure: Effects on seismic attributes. *Geophysics*, *65*, 1769–1779. https://doi.org/10.1190/1.1444861

Cavelan, A., Boussafir, M., Rozenbaum, O., & Laggoun-Défarge, F. (2019). Organic petrography and pore structure characterization of low-mature and gas-mature marine organic-rich mudstones: Insights into porosity controls in gas shale systems. *Marine and Petroleum Geology*, *103*, 331–350. https://doi.org/10.1016/j.marpetgeo.2019.02.027

Chen, Z., & Jiang, C. (2016). A revised method for organic porosity estimation in shale reservoirs using Rock-Eval data: Example from Duvernay Formation in the Western Canada Sedimentary Basin. *AAPG Bulletin*, *100*, 405–422. https://doi.org/10.1306/08261514173

Chen, Z., Wang, T., Liu, Q., Zhang, S., & Zhang, L. (2015). Quantitative evaluation of potential organic-matter porosity and hydrocarbon generation and expulsion from mudstone in continental lake basins: A case study of Dongying sag, eastern China. *Marine and Petroleum Geology*, *66*, 906–924. https://doi.org/10.1016/j.marpetgeo.2015.07.027

Cobbold, P. R., & Rossello, E. A. (2003). Aptian to recent compressional deformation, foothills of the Neuquén Basin, Argentina. *Marine and Petroleum Geology*, *20*, 429–443. https://doi.org/10.1016/S0264-8172(03)00077-1

Cobbold, P. R., Zanella, A., Rodrigues, N., & Løseth, H. (2013). Bedding-parallel fibrous veins (beef and cone-in-cone): Worldwide occurrence and possible significance in terms of fluid overpressure, hydrocarbon generation and mineralization. *Marine and Petroleum Geology*, *43*, 1–20. https://doi.org/10.1016/j.marpetgeo.2013.01.010

Comerio, M., Fernández, D. E., & Pazos, P. J. (2018). Sedimentological and ichnological characterization of muddy storm related deposits: The upper Hauterivian ramp of the Agrio Formation in the Neuquén Basin, Argentina. *Cretaceous Research*, *85*, 78–94. https://doi.org/10.1016/j.cretres.2017.11.024

Comerio, M., Fernández, D. E., Rendtorff, N., Cipollone, M., Zalba, P. E., & Pazos, P. J. (2020). Depositional and postdepositional processes of an oil-shale analog at the microstructure scale: The Lower Cretaceous Agrio Formation, Neuquén Basin, northern Patagonia. *AAPG Bulletin*, *104*, 1679–1705. https://doi.org/10.1306/04082017419

Couzens-Schultz, B., Axon, A., & Azbel, K. (2013). *Pore pressure prediction in unconventional resources*. In IPTC Paper 16849 presented at the International Petroleum Technology Conference, Beijing, China, 26–28 March.

Cruz, C. E., Boll, A., Gómez Omil, R., Martínez, E. A., Arregui, C., Gulisano, C., Laffitte, G., & Villar, H. J. (2002). Hábitat de hidrocarburos y sistemas de carga Los Molles y Vaca Muerta en el sector central de la Cuenca Neuquina, Argentina. In *Congreso de Exploración y Desarrollo de Hidrocarburos* (No. 5).

Cruz, C. E., Villar, H. J., & Muñoz, N. G. (1996). Los sistemas petroleros del Grupo Mendoza en la Fosa de Chos Malal. Cuenca Neuquina, Argentina. In *13° Congreso Geológico Argentino y 3° Congreso de Exploración de Hidrocarburos, Actas 1*, AGA–IAPG, Buenos Aires, Argentina, 13–18 October (pp. 45–60).

Cuervo, S., Lombardo, E., Vallejo, D., Crousse, L., Hernandez, C., & Mosse, L. (2016). Towards a simplified petrophysical model for the Vaca Muerta Formation. In *Unconventional Resources Technology Conference (URTeC)*, San Antonio, Texas, 1–3 August 2016 (pp. 778–796).

Curiale, J. A., & Curtis, J. B. (2016). Organic geochemical applications to the exploration for source-rock reservoirs–A review. *Journal of Unconventional Oil and Gas Resources*, *13*, 1–31. https://doi.org/10.1016/j.juogr.2015.10.001

Dembicki, H. Jr (2009). Three common source rock evaluation errors made by geologists during prospect or play appraisals. *AAPG Bulletin*, *93*, 341–356. https://doi.org/10.1306/10230808076

Deming, D. (1989). Application of bottom-hole temperature corrections in geothermal studies. *Geothermics*, *18*, 775–786. https://doi.org/10.1016/0375-6505(89)90106-5

Desjardins, P., Fantín, M., González Tomassini, F., Reijenstein, H., Sattler, F., Dominguez, R. F., Kietzmann, D., Leanza, H. A., Bande, A., Benoit, S., Borgnia, M., Vittore, F., Gil, G., Simo, T., & Minisini, D. (2016). Capítulo 2: Estratigrafía Sísmica Regional. In G. González (Ed.), *Transecta Regional de la Formación Vaca Muerta (IAPG), Buenos Aires*.

Dominguez, F., Noguera, I. L., Continanzia, M. J., Mykietiuk, K., Ponce, C., Pérez, G., Guerello, R., Caneva, M., Di Benedetto, M., & Cristallini, E. (2016). Organic-rich stratigraphic units in the Vaca Muerta formation, and their distribution and characterization in the Neuquén Basin (Argentina). *Unconventional Resources Technology Conference (URTEC)*.

Dominguez, R. F., & Di Benedetto, M. (2019). Understanding 3-D distribution of organic-rich units in the Vaca Muerta Formation. In *Unconventional Resources Technology Conference*, Denver, Colorado, 22–24 July 2019 (pp. 5114–5128).

Doré, A. G., & Jensen, L. N. (1996). The impact of late Cenozoic uplift and erosion on hydrocarbon exploration: Offshore Norway and some other uplifted basins. *Global and Planetary Change*, *12*, 415–436. https://doi.org/10.1016/0921-8181(95)00031-3

Ejofodomi, E., Baihly, J. D., Malpani, R., Altman, R. M., Huchton, T. J., Welch, D., & Zieche, J. (2011). Integrating all available data to improve production in the Marcellus Shale. In *North American Unconventional Gas Conference and Exhibition*. Society of Petroleum Engineers.

Espitalié, J., Deroo, G., & Marquis, F. (1986). La pyrolyse Rock-Eval et ses applications. Troisième partie. *Revue de l'institut Français du Pétrole*, *41*(1), 73–89. https://doi.org/10.2516/ogst:1986003

Franzese, J. R., & Spalletti, L. A. (2001). Late Triassic continental-extension in southwestern Gondwana: Tectonic segmentation and pre-breakup rifting. *Journal of South American Earth Sciences*, *14*, 257–270.

Gao, J., Zhang, J.-K., He, S., Zhao, J.-X., He, Z.-L., Wo, Y.-J., Feng, Y.-X., & Li, W. (2019). Overpressure generation and evolution in Lower Paleozoic gas shales of the Jiaoshiba region, China: Implications for shale gas accumulation. *Marine and Petroleum Geology*, *102*, 844–859. https://doi.org/10.1016/j.marpetgeo.2019.01.032

Gibson, R. G., & Bentham, P. A. (2003). Use of fault-seal analysis in understanding petroleum migration in a complexly faulted anticlinal trap, Columbus Basin, offshore Trinidad. *AAPG Bulletin*, *87*, 465–478.

Gómez Omil, R., Caniggia, J., & Borghi, P. (2014). La Formación Vaca Muerta en la faja plegada de Neuquén y Mendoza. Procesos que controlaron su madurez. *IX Congreso de Exploración y Desarrollo de Hidrocarburos*. Actas DVD (pp. 71–96).

Groeber, P. (1946). Observaciones geológicas a lo largo del meridiano 70° 1. Hoja Chos Malal. *Revista de la Asociación Geológica Argentina*, *1*, 177–208.

Grohmann, S., Fietz, W. S., Nader, F. H., Romero-Sarmiento, M. F., Baudin, F., & Littke, R. (2021). Characterization of Late Cretaceous to Miocene source rocks in the Eastern Mediterranean Sea: An integrated numerical approach of stratigraphic forward modelling and petroleum system modelling. *Basin Research*, *33*, 846–874. https://doi.org/10.1111/bre.12497

Hackley, P. C., & Cardott, B. J. (2016). Application of organic petrography in North American shale petroleum systems: A review. *International Journal of Coal Geology*, *163*, 8–51. https://doi.org/10.1016/j.coal.2016.06.010

Hantschel, T., & Kauerauf, A. I. (2009). *Fundamentals of basin and petroleum systems modeling* (p. 476). Springer.

Hao, F., Li, S., Sun, Y., & Zhang, Q. (1996). Characteristics and origin of the gas and condensate in the Yinggehai Basin, offshore South China Sea: Evidence for effects of overpressure on petroleum generation and migration. *Organic Geochemistry*, *24*, 363–375. https://doi.org/10.1016/0146-6380(96)00009-5

Hazra, B., Wood, D. A., Mani, D., Singh, P. K., & Singh, A. K. (2019). *Evaluation of shale source rocks and reservoirs* (p. 139). Springer.

Horton, B. K. (2018). Sedimentary record of Andean mountain building. *Earth-Science Reviews*, *178*, 279–309.

Horton, B. K., Fuentes, F., Boll, A., Starck, D., Ramirez, S. G., & Stockli, D. F. (2016). Andean stratigraphic record of the transition from backarc extension to orogenic shortening: A case study from the northern Neuquén Basin, Argentina. *Journal of South American Earth Sciences*, *71*, 17–40. https://doi.org/10.1016/j.jsames.2016.06.003

Howell, J. A., Schwarz, E., Spalletti, L. A., & Veiga, G. D. (2005). The Neuquén Basin: An overview. In G. D. Veiga, L. A. Spalletti, J. A. Howell, & E. Schwarz (Eds.), *The Neuquén Basin: A case study in sequence stratigraphy and basin dynamics* (Vol. 252, pp. 1–14). Geological Society, London, Special Publications.

Hunt, J. M. (1990). Generation and migration of petroleum from abnormally pressured fluid compartments. *AAPG Bulletin*, *74*, 1–12.

Jorgensen, L., López Pezé, A., & Pisani, F. (2013). *Caracterización de la Formación Los Molles como reservorio de tipo Shale Gas en el ámbito Norte de la Dorsal de Huincul, Cuenca Neuquina, Argentina, Mostrando su analogía con reservorio de Shale Gas probado en EEUU*. Society of Petroleum Engineers.

Karg, H., & Littke, R. (2020). Tectonic control on hydrocarbon generation in the northwestern Neuquén Basin, Argentina. *AAPG Bulletin*, *104*, 2173–2208. https://doi.org/10.1306/05082018171

Katz, B. J. (Ed.) (1995). Petroleum source rocks—An introductory overview. In: *Petroleum source rocks* (pp. 1–8). Springer-Verlag; Berlin.

Katz, B. J., & Arango, I. (2018). Organic porosity: A geochemist's view of the current state of understanding. *Organic Geochemistry*, *123*, 1–16. https://doi.org/10.1016/j.orggeochem.2018.05.015

Katz, B. J., & Lin, F. (2021). Consideration of the limitations of thermal maturity with respect to vitrinite reflectance, T_{max}, and other proxies. *AAPG Bulletin*, *105*(4), 695–720.

Kietzmann, D. A., Ambrosio, A. L., Suriano, J., Alonso, M. S., González Tomassini, F., Depine, G., & Repol, D. (2016). The Vaca Muerta-Quintuco system (Tithonian–Valanginian) in the Neuquén basin, Argentina: A view from the outcrops in the Chos Malal fold and thrust belt. *AAPG Bulletin*, *100*, 743–771. https://doi.org/10.1306/02101615121

Ko, L. T., Loucks, R. G., Ruppel, S. C., Zhang, T., & Peng, S. (2017). Origin and characterization of Eagle Ford pore networks in the south Texas Upper Cretaceous shelf. *AAPG Bulletin*, *101*, 387–418. https://doi.org/10.1306/08051616035

Kozlowski, S., Cruz, C. E., & Sylwan, C. (1998). Modelo exploratorio en la faja corrida de la Cuenca Neuquina, Argentina. *Boletín de Informaciones Petroleras*, *55*, 4–23.

Krim, N., Tribovillard, N., Riboulleau, A., Bout-Roumazeilles, V., Bonnel, C., Imbert, P., Aubourg, C., Hoareau, G., & Fasentieux, B. (2019). Reconstruction of palaeoenvironmental conditions of the Vaca Muerta Formation in the southern part of the Neuquén Basin (Tithonian-Valanginian): Evidences of initial short-lived development of anoxia. *Marine and Petroleum Geology*, *103*, 176–201. https://doi.org/10.1016/j.marpetgeo.2019.02.011

Lampe, C., Kornpihl, K., Sciamanna, S., Zapata, T., Zamora, G., & Varadé, R. (2006). Petroleum systems modeling in tectonically complex areas—A 2D migration study from the Neuquen Basin, Argentina. *Journal of Geochemical Exploration*, *89*, 201–204.

Law, B. E., & Dickinson, W. W. (1985). Conceptual model for origin of abnormally pressured gas accumulations in low-permeability reservoirs. *AAPG Bulletin*, *69*, 1295–1304.

Law, B. E. & Spencer, C. W. (1998). Abnormal pressures in hydrocarbon environments. In: B. E. Law, G. F. Ulmishek & V. I. Slavin (Eds.), *Abnormal pressures in hydrocarbon environments* (Vol. 70, pp. 1–11). AAPG Memoir.

Leanza, H. A. (2003). *Las sedimentitas huitrinianas y rayosianas (Cretácico inferior) en el ámbito central y meridional de la cuenca Neuquina, Argentina*. Servicio Geológico Minero Argentino, Serie Contribuciones Técnicas, Geología 2 (p. 31).

Leanza, H. A., & Hugo, C. A. (2001). Hoja Geológica 3969-I: Zapala: Programa Nacional de Cartas Geológicas de la República Argentina 1:250.000. *Instituto de Geología y Recursos Minerales Boletín 275* (p. 128).

Legarreta, L., & Uliana, M. A. (1991). Jurassic–marine oscillations and geometry of back-arc basin fill, Central Argentina Andes. In D. I. M. McDonald (Ed.), *Sedimentation, tectonics and eustacy: Sea level changes at active plate margins* (pp. 429–450). Blackwell Scientific Publications.

Legarreta, L., ViIIar, H. J., Cruz, C. E., Laffitte, G. A., & Varadé, R. (2008). Revisión integrada de los sistemas generadores, estilos de migración-entrampamiento, y volumetría de hidrocarburos en los distritos productivos de la cuenca Neuquina, Argentina. In C. E. Cruz, J. F. Rodríguez, J. J. Hechern, & H. J. Villar (Eds.), *Sistemas Petroleros de las Cuencas Andinas* (pp. 79–108). Instituto Argentino del Petróleo y el Gas.

Legarreta, L., & Villar, H. J. (2011). Geological and geochemical keys of the potential shale resources, Argentina basins. *AAPG Search and Discovery Article* 80196. Accessed November 7, 2011. http://www.searchanddiscovery.com/pdfz/documents/2011/80196legarreta/ndx_legarreta.pdf.html

Legarreta, L., & Villar, H. J. (2012). Las facies generadoras de hidrocarburos de la Cuenca Neuquina. *Petrotecnia*, 14–39.

Legarreta, L., & Villar, H. J. (2015). The Vaca Muerta Formation (Late Jurassic-Early Cretaceous), Neuquén Basin, Argentina: Sequences, facies and source rock characteristics. In *Extended Abstracts*.

Liu, B., Schieber, J., & Mastalerz, M. (2017). Combined SEM and reflected light petrography of organic matter in the New Albany Shale (Devonian-Mississippian) in the Illinois Basin: A perspective on organic pore development with thermal maturation. *International Journal of Coal Geology*, *184*, 57–72. https://doi.org/10.1016/j.coal.2017.11.002

Löhr, S., Baruch, E., Hall, P., & Kennedy, M. (2015). Is organic pore development in gas shales influenced by the primary porosity and structure of thermally immature organic matter? *Organic Geochemistry*, *87*, 119–132. https://doi.org/10.1016/j.orggeochem.2015.07.010

Loucks, R. G., Reed, R. M., Ruppel, S. C., & Jarvie, D. M. (2009). Morphology, genesis, and distribution of nanometer-scale pores in siliceous mudstones of the Mississippian Barnett Shale. *Journal of Sedimentary Research*, *79*, 848–861. https://doi.org/10.2110/jsr.2009.092

Małachowska, A., Mastalerz, M., Hampton, L., Hupka, J., & Drobniak, A. (2019). Origin of bitumen fractions in the Jurassic-early Cretaceous Vaca Muerta Formation in Argentina: Insights from organic petrography and geochemical techniques. *International Journal of Coal Geology*, *205*, 155–165. https://doi.org/10.1016/j.coal.2018.11.013

Martínez, M. A., Prámparo, M. B., Quattrocchio, M. E., & Zavala, C. A. (2008). Depositional environments and hydrocarbon potential of the Middle Jurassic Los Molles Formation, Neuquén Basin, Argentina: Palynofacies and organic geochemical data. *Andean Geology*, *35*, 279–305. https://doi.org/10.5027/andgeoV35n2-a05

Mastalerz, M., Drobniak, A., & Tankiewicz, A. B. (2018). Origin, properties, and implications of solid bitumen in source-rock reservoirs: A review. *International Journal of Coal Geology*, *195*, 14–36. https://doi.org/10.1016/j.coal.2018.05.013

McCarthy, K., Rojas, K., Niemann, M., Palmowski, D., Peters, K., & Stankiewicz, A. (2011). Basic petroleum geochemistry for source rock evaluation. *Oilfield Review*, *23*, 32–43.

McPeek, L. A. (1981). Eastern Green River basin: A developing giant gas supply from deep, overpressured Upper Cretaceous sandstones. *AAPG Bulletin*, *65*, 1078–1098.

Mei, M., Burnham, A. K., Schoellkopf, N., Wendebourg, J., & Gelin, F. (2021). Modeling petroleum generation, retention, and expulsion from the Vaca Muerta Formation, Neuquén Basin, Argentina: Part I. Integrating compositional kinetics and basin modeling. *Marine and Petroleum Geology*, *123*, 104743.

Milliken, K. L., Ko, L. T., Pommer, M., & Marsaglia, K. M. (2014). SEM Petrography of Eastern Mediterranean sapropels: Analogue data for assessing organic matter in oil and gas shales. *Journal of Sedimentary Research*, *84*, 961–974.

Milliken, K. L., Reed, R. M., McCarty, D. K., Bishop, J., Lipinski, C., Fischer, T. B., Crousse, L., & Reijenstein, H. (2019). Grain assemblages and diagenesis in the Vaca Muerta Formation (Jurassic-Cretaceous), Neuquén Basin, Argentina. *Sedimentary Geology*, *380*, 45–64. https://doi.org/10.1016/j.sedgeo.2018.11.007

Milliken, K. L., Rudnicki, M., Awwiller, D. N., & Zhang, T. (2013). Organic matter–hosted pore system, Marcellus formation (Devonian), Pennsylvania. *AAPG Bulletin*, *97*, 177–200. https://doi.org/10.1306/07231212048

Mitchum, R. M. Jr, & Uliana, M. A. (1985). Seismic stratigraphy of carbonate depositional sequences, Upper Jurassic-Lower Cretaceous, Neuquén Basin, Argentina. In O. R. Berg, & D. G. Woolverton (Eds.), *Seismic stratigraphy II: An integrated approach to hydrocarbon exploration* (pp. 255–274). American Association Petroleum Geologists, Memoir 39.

Modica, C. J., & Lapierre, S. G. (2012). Estimation of kerogen porosity in source rocks as a function of thermal transformation: Example from the Mowry Shale in the Powder River Basin of Wyoming estimation of kerogen porosity as a function of thermal transformation. *AAPG Bulletin*, *96*, 87–108. https://doi.org/10.1306/04111110201

Naipauer, M., Comerio, M., Lescano, M. A., Vennari, V. V., Aguirre-Urreta, B., Pimentel, M. M., & Ramos, V. A. (2020). The Huncal Member of the Vaca Muerta Formation, Neuquén Basin of Argentina: Insight into biostratigraphy, structure, U-Pb detrital zircon ages and provenance. *Journal of South American Earth Sciences*, *100*, 102567. https://doi.org/10.1016/j.jsames.2020.102567

Neuzil, C. E., & Pollock, D. W. (1983). Erosional unloading and fluid pressures in hydraulically "tight" rocks. *The Journal of Geology*, *91*, 179–193. https://doi.org/10.1086/628755

Nunn, J. A. (2012). Burial and thermal history of the Haynesville Shale: Implications for overpressure, gas generation, and natural hydrofracture. *Gulf Coast Association of Geological Society Journal*, *1*, 81–96.

Olivera, D. E., Martínez, M. A., Zavala, C., Di Nardo, J. E., & Otharán, G. (2020). New contributions to the palaeoenvironmental framework of the Los Molles Formation (Early-to-Middle Jurassic), Neuquén Basin, based on palynological data. *Facies*, *66*, 1–21. https://doi.org/10.1007/s10347-020-00607-8

Ortiz, A. C., Crousse, L., Bernhardt, C., Vallejo, D., & Mosse, L. (2020). Reservoir properties: Mineralogy, porosity, and fluid types. In D. Minisini, M. Fantín, I. Lanusse Noguera, & H. Leanza (Eds.), *Integrated geology of unconventionals: The case of the Vaca Muerta play, Argentina*. AAPG Memoir 121 (pp. 329–350).

Osborne, M. J., & Swarbrick, R. E. (1997). Mechanisms for generating overpressure in sedimentary basins: A reevaluation. *AAPG Bulletin*, *81*, 1023–1041.

Otharán, G., Zavala, C., Arcuri, M., Di Meglio, M., Zorzano, A., Marchal, D., & Koller, G. (2020). Análisis de facies de fangolitas bituminosas asociadas a flujos fluidos de fango. Sección inferior de la Formación Vaca Muerta (Tithoniano), Cuenca Neuquina central, Argentina. *Andean Geology*, *47*, 384–417.

Passey, Q. R., Bohacs, K., Esch, W. L., Klimentidis, R., & Sinha, S. (2010). From oil-prone source rock to gas-producing shale reservoir-geologic and petrophysical characterization of unconventional shale gas reservoirs. In *International Oil and Gas Conference and Exhibition*, Beijing, China, June 8–10, 2010, SPE Paper 131350 (p. 29).

Pazos, P. J., Comerio, M., Fernández, D. E., Gutiérrez, C., Estebenet, M. C. G., & Heredia, A. M. (2020). Sedimentology and Sequence Stratigraphy of the Agrio Formation (Late Valanginian-Earliest Barremian) and the Closure of the Mendoza Group to the North of the Huincul High. In: A. Folguera & D. Kietzmann (Eds.), *Opening and Closure of the Neuquén Basin in the Southern Andes* (pp. 237–265). Springer.

Peters, K. E. (1986). Guidelines for evaluating petroleum source rock using programmed pyrolysis. *AAPG Bulletin*, *70*, 318–329.

Peters, K. E., Burnham, A. K., Walters, C. C., & Schenk, O. (2018). Guidelines for kinetic input to petroleum system models from open-system pyrolysis. *Marine and Petroleum Geology*, *92*, 979–986. https://doi.org/10.1016/j.marpetgeo.2017.11.024

Peters, K. E. & Cassa, M. R. (1994). Applied source rock geochemistry. In: L. B. Magoon & W. G. Dow (Eds.), *The Petroleum System—From Source to Trap* (Vol. 60, pp. 93–117). American Association of Petroleum Geologists Memoir.

Peters, K. E., Schenk, O., Hosford Scheirer, A., Wygrala, B., & Hantschel, T. (2017). Basin and petroleum system modeling, Chapter 11. In C. S. Hsu & P. R. Robinson (Eds.), *Handbook of petroleum technology* (2nd edn., pp. 381–417). Springer.

Petersen, H. I., Sanei, H., Gelin, F., Loustaunau, E., & Despujols, V. (2020). Kerogen composition and maturity assessment of a solid bitumen-rich and vitrinite-lean shale: Insights from the Upper Jurassic Vaca Muerta Shale, Argentina. *International Journal of Coal Geology*, *229*, 103575.

Pommer, M., & Milliken, K. (2015). Pore types and pore-size distributions across thermal maturity, Eagle Ford Formation, southern Texas. *AAPG Bulletin*, *99*, 1713–1744. https://doi.org/10.1306/03051514151

Ramdhan, A. M., & Goulty, N. R. (2010). Overpressure-generating mechanisms in the Peciko field, lower Kutai Basin, Indonesia. *Petroleum Geoscience*, *16*, 367–376. https://doi.org/10.1144/1354-079309-027

Ramos, V. A., Mosquera, A., Folguera, A., & García Morabito, E. (2011). Evolución tectónica de los Andes y del Engolfamiento Neuquino adyacente. In *Geología y Recursos Naturales de la Provincia de Neuquén. Relatorio del VXIII Congreso Geológico Argentino, Buenos Aires* (pp. 335–348).

Reed, R. M., & Loucks, R. G. (2015). Low-thermal-maturity (0.7% VR) mudrock pore systems: Mississippian Barnett Shale, southern Fort Worth Basin. *Gulf Coast Association of Geological Society*, *4*, 15–28.

Rocha, E., Brisson, I., & Fasola, M. (2018). Modelado de Sistemas petroleros a lo largo de la faja plegada de cuenca neuquina. In M. Gardini, M. L. Ayoroa, C. E. Cruz, M. Gomez, M. Limeres, P. Malone, R. Manceda, G. Peroni, & H. Villar (Eds.), *X Congreso de Exploración y Desarrollo de Hidrocarburos*, Mendoza, Argentina, 5–9 November (pp. 301–314).

Rodrigues, N., Cobbold, P. R., Loseth, H., & Ruffet, G. (2009). Widespread bedding-parallel veins of fibrous calcite ('beef') in a mature source rock (Vaca Muerta Fm, Neuquén Basin, Argentina): Evidence for overpressure and horizontal compression. *Journal of the Geological Society*, *166*, 695–709. https://doi.org/10.1144/0016-76492008-111

Roduit, N. (2008). JMICROVISION version 1.2.7: Image analysis toolbox for measuring and quantifying components of high definition images. Accessed November 1, 2012. http://www.jmicrovision.com

Rojas Vera, E. A., Folguera, A., Zamora Valcarce, G., Giménez, M., Ruiz, F., Martínez, P., Bottesi, G., & Ramos, V. A. (2010). Neogene to Quaternary extensional reactivation of a fold and thrust belt: The Agrio belt in the Southern Central Andes and its relation to the Loncopue trough (38°–39° S). *Tectonophysics*, *492*, 279–294.

Rojas Vera, E. R., Mescua, J., Folguera, A., Becker, T., Sagripanti, L., Fennell, L., Orts, D., & Ramos, V. A. (2015). Evolution of the Chos Malal and Agrio fold and thrust belts, Andes of Neuquén: Insights from structural analysis and apatite fission track dating. *Journal of South American Earth Sciences*, *64*, 418–433. https://doi.org/10.1016/j.jsames.2015.10.001

Romero-Sarmiento, M.-F., Ducros, M., Carpentier, B., Lorant, F., Cacas, M.-C., Pegaz-Fiornet, S., Wolf, S., Rohais, S., & Moretti, I. (2013). Quantitative evaluation of TOC, organic porosity and gas retention distribution in a gas shale play using petroleum system modeling: Application to the Mississippian Barnett Shale. *Marine and Petroleum Geology*, *45*, 315–330. https://doi.org/10.1016/j.marpetgeo.2013.04.003

Romero-Sarmiento, M. F., Ramiro-Ramirez, S., Berthe, G., Fleury, M., & Littke, R. (2017). Geochemical and petrophysical source rock characterization of the Vaca Muerta Formation, Argentina: Implications for unconventional petroleum resource estimations. *International Journal of Coal Geology*, *184*, 27–41. https://doi.org/10.1016/j.coal.2017.11.004

Romero-Sarmiento, M. F., Rouzaud, J. N., Bernard, S., Deldicque, D., Thomas, M., & Littke, R. (2014). Evolution of Barnett Shale organic carbon structure and nanostructure with increasing maturation. *Organic Geochemistry*, *71*, 7–16. https://doi.org/10.1016/j.orggeochem.2014.03.008

Rouquerol, J., Avnir, D., Fairbridge, D. H., Everett, J. H., Pernicone, N., Ramsay, J. D. F., Sing, K. S. W., & Unger, F. (1994). Recommendations for the characterization of porous solids. *Pure and Applied Chemistry*, *68*, 1739–1758.

Sagasti, G., Foster, M., Hryb, D., Ortiz, A., & Lazzari, V. (2014). Understanding geological heterogeneity to customize field development: An example from the Vaca Muerta unconventional play, Argentina. In *Unconventional Resources Technology Conference*, Denver, Colorado (pp. 797–816).

Sánchez, N. P., Coutand, I., Turienzo, M., Lebinson, F., Araujo, V., & Dimieri, L. (2018). Tectonic evolution of the Chos Malal fold-and-thrust belt (Neuquén Basin, Argentina) from (U-Th)/He and fission track thermochronometry. *Tectonics*, *37*, 1907–1929. https://doi.org/10.1029/2018TC004981

Scasso, R. A., Alonso, M. S., Lanes, S., Villar, H. J., & Laffitte, G. (2005). Geochemistry and petrology of a Middle Tithonian limestone-marl rhythmite in the Neuquén Basin, Argentina: Depositional and burial history. In G. D. Veiga, L. A. Spalletti, J. A. Howell, & E. Schwarz (Eds.), *The Neuquén Basin, Argentina: A case study in sequence stratigraphy and basin dynamics* (Vol. 252, pp. 207–229). Geological Society, London, Special Publication.

Schieber, J. (2010). Common themes in the formation and preservation of intrinsic porosity in shales and mudstones—Illustrated with examples across the Phanerozoic. In *Society of Petroleum Engineers Unconventional Gas Conference*, Pittsburgh, Pennsylvania, February 23–25, 2010, SPE-132370-MS (p. 10).

Schieber, J. (2013). SEM observations on ion-milled samples of Devonian black shales from Indiana and New York: The petrographic context of multiple pore types. In W. Camp, E. Diaz, & B. Wawak (Eds.), *Electron microscopy of shale hydrocarbon reservoirs*. AAPG Memoir 102 (pp. 153–171).

Schieber, J., Lazar, R., Bohacs, K., Klimentidis, B., Ottmann, J., & Dumitrescu, M. (2016). An SEM study of porosity in the Eagle Ford Shale of Texas – Pore types and porosity distribution in a depositional and sequence stratigraphic context. *AAPG Memoir*, *110*, 153–172.

Shanley, K. W., & Cluff, R. M. (2015). The evolution of pore-scale fluid-saturation in low-permeability sandstone reservoirs. *AAPG Bulletin*, *99*, 1957–1990. https://doi.org/10.1306/03041411168

Spacapan, J. B., D'Odorico, A., Palma, O., Galland, O., Vera, E. R., Ruiz, R., Leanza, H. A., Medialdea, A., & Manceda, R. (2020). Igneous petroleum systems in the Malargüe fold and thrust belt, Río Grande Valley area, Neuquén Basin, Argentina. *Marine and Petroleum Geology*, *111*, 309–331. https://doi.org/10.1016/j.marpetgeo.2019.08.038

Spacapan, J. B., Palma, J. O., Galland, O., Manceda, R., Rocha, E., D'Odorico, A., & Leanza, H. A. (2018). Thermal impact of igneous sill-complexes on organic-rich formations and implications for petroleum systems: A case study in the northern Neuquén Basin, Argentina. *Marine and Petroleum Geology*, *91*, 519–531. https://doi.org/10.1016/j.marpetgeo.2018.01.018

Spalletti, L., Franzese, J., Matheos, S., & Schwarz, E. (2000). Sequence stratigraphy of tidally-dominated carbonate-siliciclastic ramp; the Tithonian of the southern Neuquén Basin, Argentina. *Journal of the Geological Society of London*, *157*, 433–446.

Stipanicic, P. N., Rodrigo, F., Baulies, O. L., & Martínez, C. G. (1968). Las Formaciones presenonianas en el denominado Macizo Nordpatagónico y regiones adyacentes. *Revista de la Asociación Geológica Argentina*, *23*, 67–98.

Swarbrick, R. E., Osborne, M. J., & Yardley, G. S. (2002). Comparison of overpressure magnitude resulting 809 from the main generating mechanisms. In A. R. Huffman & G. L. Bowers (Eds.), *Pressure regimes in 810 sedimentary basins and their prediction*. AAPG Memoir 76 (pp. 1–12).

Sweeney, J. J., & Burnham, A. K. (1990). Evaluation of a simple model of vitrinite reflectance based on chemical kinetics. *AAPG Bulletin*, *74*, 1559–1570.

Sylwan, C. (2014). Source rock properties of Vaca Muerta Formation, Neuquina Basin, Argentina. Simposio de Recursos No Convencionales. Ampliando el Horizonte Energético. *IX° Congreso de Exploración y Desarrollo de Hidrocarburos* (pp. 365–386).

Tingay, M. R., Hillis, R. R., Swarbrick, R. E., Morley, C. K., & Damit, A. R. (2009). Origin of overpressure and pore-pressure prediction in the Baram province, Brunei. *AAPG Bulletin*, *93*, 51–74. https://doi.org/10.1306/08080808016

Tissot, B. P., & Welte, D. H. (1984). From kerogen to petroleum. In B. P. Tissot & D. H. Welte (Eds.), *Petroleum formation and occurrence* (pp. 160–198). Springer.

Tomassini, F. G., Smith, L., Rodriguez, M. J., Kietzmann, D., Jausoro, I., Floridia, M. A., Cipollone, M., Caneiro, A., Epele, B., Santillán, N., & Medina, F. (2019). Semi-quantitative SEM analysis of the Vaca Muerta Formation and its impact on reservoir characterization, Neuquén Basin, Argentina. In *Unconventional Resources Technology Conference (URTeC)*, Denver, Colorado, 22–24 July 2019 (pp. 3175–3188).

Tunik, M. A., Folguera, A., Naipauer, M., Pimentel, M., & Ramos, V. A. (2010). Early uplift and orogenic deformation in the Neuquén Basin: Constraints on the Andean uplift from U-Pb and Hf isotopic

data of detrital zircons. *Tectonophysics*, *489*, 258–273. https://doi.org/10.1016/j.tecto.2010.04.017

Uliana, M., & Legarreta, L. (1993). Hydrocarbon habitat in a Triassic-to-Cretaceous Sub-Andean setting: Neuquén Basin, Argentina. *Journal of Petroleum Geology*, *16*, 397–420.

Urien, M. C., & Zambrano, J. J. (1994). Petroleum systems in the Neuquén Basin, Argentina. In L. B. Magoon & W. G. Dow (Eds.), *The petroleum system–From source to trap*. AAPG Memoir 60 (pp. 513–534).

Veiga, R. D., Vergani, G. D., Brissón, I. E., Macellari, C. E., & Leanza, H. A. (2020). The Neuquén Super Basin. *AAPG Bulletin*, *104*, 2521–2555. https://doi.org/10.1306/09092020023

Vennari, V. V., Lescano, M., Naipauer, M., Aguirre-Urreta, M. B., Concheyro, A., Schaltegger, U., Armstrong, R., Pimentel, M., & Ramos, V. A. (2014). New constraints on the Jurassic-Cretaceous boundary in the High Andes using high-precision U-Pb data. *Gondwana Research*, *26*, 374–385. https://doi.org/10.1016/j.gr.2013.07.005

Vergani, G., Arregui, C., Carbone, O., Leanza, H. A., Danieli, J. C., & Vallés, J. M. (2011). Sistemas petroleros y tipos de entrampamientos en la Cuenca Neuquina. In *Geologia y Recursos Naturales de la Provincia de Neuquén: XVIII Congreso Geológico Argentino* (pp. 645–656).

Vergani, G. D., Tankard, A. J., Belotti, H. J., & Welsink, H. J. (1995). Tectonic evolution and paleogeography of the Neuquén Basin, Argentina. In A. J. Tankard, S. R. Suárez, & H. J. Welsink (Eds.), *Petroleum Basins of South America*. AAPG Memoir 62 (pp. 383–402).

Wang, F. P., & Gale, J. F. (2009). Screening criteria for shale-gas systems. *Gulf Coast Association of Geological Societies Transactions*, *59*, 779–793.

Wang, G. (2020). Deformation of organic matter and its effect on pores in mud rocks. *AAPG Bulletin*, *104*, 21–36. https://doi.org/10.1306/04241918098

Waples, D., & Tobey, M. H. (2015). Like space and time, transformation ratio is curved. Search and Discovery Article #41713 (2015) Posted October 26, 2015.

Weaver, C. E. (1931). Paleontology of the Jurassic and Cretaceous of West Central Argentina. *Memoirs of the University of Washington* (Vol. *1*, p. 469). University of Washington Press.

Williams, K. E., & Madatov, A. G. (2005). Analysis of pore pressure compartments in extensional basins. In *25th Annual, GCSSEPM Foundation Annual Bob F. Perkins Research Conference Proceedings: Petroleum Systems of Divergent Continental Margin Basins* (pp. 862–890).

Wilson, R. D., & Schieber, J. (2016). The influence of primary and secondary sedimentary features on reservoir quality: Examples from the Geneseo Formation of New York, U.S.A. In T. Olson (Ed.), *Imaging unconventional reservoir pore systems*. AAPG Memoir 112 (pp. 167–184).

Wygrala, B. P. (1989). Integrated study of an oil field in the southern Po Basin, Northern Italy. *Berichte Kernforschungsanlage Jülich*, *2313*, 217.

Zamora Valcarce, G., Rapalini, A. E., & Spagnuolo, C. M. (2007). Reactivación de estructuras cretácicas durante la deformación miocena, Faja Plegada del Agrio, Neuquén. *Revista de la Asociación Geológica de Argentina*, *62*, 299–307.

Zamora Valcarce, G. Z., Zapata, T., & Ramos, V. A. (2011). La faja plegada y corrida del Agrio. In *Relatorio Geología y Recursos Naturales de la provincia del Neuquén* (pp. 367–374).

Zanella, A., Cobbold, P. R., Ruffet, G., & Leanza, H. A. (2015). Geological evidence for fluid overpressure, hydraulic fracturing and strong heating during maturation and migration of hydrocarbons in Mesozoic rocks of the northern Neuquén Basin, Mendoza Province, Argentina. *Journal of South American Earth Sciences*, *62*, 229–242. https://doi.org/10.1016/j.jsames.2015.06.006

Zapata, T., & Folguera, A. (2005). Tectonic evolution of the Andean fold and thrust belt of the southern Neuquén Basin, Argentina. In: G. D. Veiga, L. A. Spalletti, J. A. Howell, & E. Schwarz (Eds.), *The Neuquén Basin: A case study in sequence stratigraphy and basin dynamics* (Vol. 252, pp. 37–56). The Geological Society, Special Publication.

SUPPORTING INFORMATION

Additional supporting information may be found online in the Supporting Information section.

How to cite this article: Spacapan, J. B., Comerio, M., Brisson, I., Rocha, E., Cipollone, M., & Hidalgo, J. C. (2021). Integrated source rock evaluation along the maturation gradient. Application to the Vaca Muerta Formation, Neuquén Basin of Argentina. *Basin Research*, 00, 1–29. https://doi.org/10.1111/bre.12599